J. Fluid Mech. (1997), *vol.* 334, *pp.* 157–188

Fully developed travelling wave solutions and bubble formation in fluidized beds

By B. J. GLASSER†, I. G. KEVREKIDIS AND S. SUNDARESAN
Department of Chemical Engineering, Princeton University, Princeton, NJ 08544, USA

(Received 12 April 1996 and in revised form 24 September 1996)

It is well known that most gas fluidized beds of particles bubble, while most liquid fluidized beds do not. It was shown by Anderson, Sundaresan & Jackson (1995), through direct numerical integration of the volume-averaged equations of motion for the fluid and particles, that this distinction is indeed accounted for by these equations, coupled with simple, physically credible closure relations for the stresses and interphase drag. The aim of the present study is to investigate how the model equations afford this distinction and deduce an approximate criterion for separating bubbling and non-bubbling systems. To this end, we have computed, making use of numerical continuation techniques as well as bifurcation theory, the one- and two-dimensional travelling wave solutions of the volume-averaged equations for a wide range of parameter values, and examined the evolution of these travelling wave solutions through direct numerical integration. It is demonstrated that whether bubbles form or not is dictated by the value of $\Omega = (\rho_s v_t^3/Ag)^{1/2}$, where ρ_s is the density of particles, v_t is the terminal settling velocity of an isolated particle, g is acceleration due to gravity and A is a measure of the particle phase viscosity. When Ω is large ($> \sim 30$), bubbles develop easily. It is then suggested that a natural scale for A is $\rho_s v_t d_p$, so that Ω^2 is simply a Froude number.

1. Introduction

Fluidized beds are frequently classified on the basis of their appearance as either *bubbling* ('aggregative') or *non-bubbling* ('particulate'). Particulate beds present a smooth appearance and expand progressively as the flow rate of fluid is increased. In contrast, aggregatively fluidized beds are traversed by rising pockets of fluid, which are reminiscent of gas bubbles in liquids. Typical examples of particulate and aggregative beds are 1 mm glass beads fluidized by water and 200 μm glass beads fluidized by ambient air, respectively. Wilhelm & Kwauk (1948) observed empirically that a fluidized bed exhibits particulate behaviour if $Fr_m = u_m^2/gd_p \ll 1$, where u_m denotes the minimum fluidization velocity and d_p is the particle diameter.

A number of theoretical studies have appeared in the literature, trying to differentiate between particulate and aggregative behaviour through linear stability analysis of the uniformly fluidized state. Such analyses have been based on (volume or ensemble) averaged equations of motion consisting of continuity and momentum equations for the two phases, with speculative closures for the effective stresses (Pigford & Baron 1965; Anderson & Jackson 1967, 1968). Garg & Pritchett (1975) showed that the

† Present address: Department of Chemical and Biochemical Engineering, Rutgers University, Piscataway, NJ 08855, USA

uniformly fluidized state can be stabilized by including in the particle phase momentum balance equation a pressure associated with the particle phase that increases sufficiently rapidly with particle concentration. The physical origin of such a stabilizing term has been the subject of much debate (Mutsers & Rietema 1977; Foscolo & Gibilaro 1984; Batchelor 1988). Experiments by Anderson & Jackson (1969) and El-Kaissy & Homsy (1976) revealed that liquid-fluidized beds of small glass beads are not uniform, but are traversed by slowly developing, rising waves; therefore one should not attempt to predict the distinction in behaviour between bubbling and non-bubbling beds on the basis of linear stability of the uniform state (Anderson, Sundaresan & Jackson 1995). Although a large number of studies have appeared on the extension of the linear stability theory to take into account the nonlinearity of the equations of motion (e.g. Fanucci, Ness & Yen 1979; Needham & Merkin 1983; Göz 1992, 1995; Harris & Crighton 1994), these analyses have not revealed any qualitative distinction between particulate and aggregative beds. (See Glasser, Kevrekidis & Sundaresan 1996, hereinafter referred to as GKS1, for a summary of these studies.)

Bubble-like structures in gas-fluidized beds have indeed been generated by numerically integrating the volume-averaged equations of motion (Pritchett, Blake & Garg 1978; Gidaspow, Syamlal & Seo 1986; Syamlal & O'Brien 1989; Kuipers, Prins & Van Swaaij 1991; Hernández & Jiménez 1991). Anderson *et al.* (1995, hereinafter referred to as ASJ) have demonstrated through numerical integration of volume-averaged equations of motion in two dimensions, assuming spatial periodicity, that these equations of motion do contain the physics needed to distinguish between bubbling and non-bubbling systems. Two-dimensional disturbances in a bed of 200 μm glass beads fluidized by ambient air were found to develop into bubble-like structures, which was not the case in a bed of 1 mm glass beads fluidized by water. Bubble-like solutions developed rapidly in the gas-fluidized bed, and they appeared to be stable two-dimensional travelling wave solutions of the equations of motion. In contrast, the two-dimensional transient solution structure continued to change in the water-fluidized bed, without settling down into any recognizable pattern even after a long period of integration. However, the origin of this difference between bubbling and non-bubbling systems is not fully resolved, and this distinction may be contained in the model equations in one of several different manners.

For example, it is possible that fully developed, two-dimensional, bubble-like structures are predicted by the model equations only for parameter values representative of bubbling beds, but not particulate beds. It is equally conceivable that fully-developed, bubble-like structures exist for both bubbling and non-bubbling systems, but their stability characteristics are different, i.e. they are stable in the case of bubbling systems and unstable in the case of non-bubbling systems. Finally, it may turn out that fully developed and linearly stable travelling wave solutions having bubble-like structure exist for both systems and that such solutions develop easily (from small disturbances which are invariably present in any system) in the case of a bubbling bed, but not a non-bubbling bed. It is important to understand which of these scenarios is the correct picture, in order to develop a proper physical basis for the manner in which the model equations afford differentiation of bubbling beds from non-bubbling ones, and to deduce a criterion to distinguish between these types of beds.

With this in mind, we have performed a detailed computational analysis of fully developed one- and two-dimensional travelling wave solutions of the volume-averaged equations of motion for fluidized suspensions. The results of such a study for parameter values that are typical of gas-fluidized beds (200 μm glass beads fluidized by ambient air, analysed by ASJ, being one of the examples) were presented in an earlier

paper, GKS1, where we showed that one-dimensional travelling wave solutions (1D-TWs) emerged from the uniform state through a Hopf bifurcation and that two-dimensional travelling wave solutions (2D-TWs) are born out of the 1D-TWs. The former has been noted in the literature previously (e.g. Needham & Merkin 1986; Göz 1992, 1993). The latter has been deduced analytically by Göz (1995) through stability analysis of small-amplitude 1D-TWs. Our computational approach allowed us to examine for the first time high-amplitude solutions and demonstrate that fully developed 2D-TWs of high amplitude have a bubble-like structure. Furthermore, the qualitative features of the bifurcation diagram were shown to be insensitive to small changes in model parameters or the closures.

In the present study, we have performed a similar bifurcation analysis for a wide range of parameter values, including those representative of 1 mm glass beads fluidized by water (a non-bubbling system analysed by ASJ) and 1 mm lead shot fluidized by water (a bubbling system). It will be shown that both bubbling and non-bubbling systems have identical bifurcation structure, and that high-amplitude 2D-TWs in both cases have a bubble-like structure. Furthermore, in every case examined in the present study, these bubble-like structures were found to be linearly stable, independent of whether the system is known to be inherently bubbling or not. It will be shown that the particle-phase velocity field in high-amplitude 2D-TWs of a bubbling bed differs from that of a non-bubbling bed in a subtle way, which influences the observability of these 2D-TWs through transient integration of the averaged equations of motion from initial states which are far away from the bubble-like solution. Thus, the distinction between bubbling and non-bubbling systems will be shown to be a feature of high-amplitude solutions, explaining why previous weakly nonlinear analyses have not been able to identify this distinction. Finally, the key parameter which distinguishes bubbling and non-bubbling systems will be identified, and an approximate criterion for this separation will be presented.

The model equations employed in the present study are summarized in §2. Section 3 is devoted to a detailed description of the results generated through computational bifurcation analysis and transient integration of the model equations for three specific fluidized bed systems which have been studied experimentally before. In §4, we discuss the role of each of the dimensionless groups appearing in the model and identify an approximate criterion for discriminating between bubbling and non-bubbling systems.

2. Model equations

The continuity and momentum balance equations for the fluid and particle phases, originally proposed by Anderson & Jackson (1967), are used in the present study. These take the form

$$\frac{\partial \phi}{\partial t} + \boldsymbol{\nabla} \cdot [\phi \boldsymbol{v}] = 0, \tag{1}$$

$$\frac{\partial (1-\phi)}{\partial t} + \boldsymbol{\nabla} \cdot [(1-\phi)\, \boldsymbol{u}] = 0, \tag{2}$$

$$\rho_s \phi \left[\frac{\partial \boldsymbol{v}}{\partial t} + \boldsymbol{v} \cdot \boldsymbol{\nabla} \boldsymbol{v} \right] = -\boldsymbol{\nabla} \cdot \boldsymbol{\sigma}_s - \phi \boldsymbol{\nabla} \cdot \boldsymbol{\sigma}_f + \boldsymbol{f} + \phi \rho_s \boldsymbol{g}, \tag{3}$$

$$\rho_f (1-\phi) \left[\frac{\partial \boldsymbol{u}}{\partial t} + \boldsymbol{u} \cdot \boldsymbol{\nabla} \boldsymbol{u} \right] = -(1-\phi)\, \boldsymbol{\nabla} \cdot \boldsymbol{\sigma}_f - \boldsymbol{f} + (1-\phi)\, \rho_f \boldsymbol{g}, \tag{4}$$

where ϕ denotes the volume fraction of particles; $\boldsymbol{v}$ and $\boldsymbol{u}$ denote the local-average velocities of the particles and the fluid; ρ_s and ρ_f are the densities; $\boldsymbol{g}$ is the specific gravity force; $\boldsymbol{f}$ is the average interaction force per unit volume of bed, exerted on the particles by the fluid, comprising interphase drag and virtual mass effects; $\boldsymbol{\sigma}_s$ and $\boldsymbol{\sigma}_f$ are the effective stress tensors for the particle and fluid phase, respectively.

Anderson *et al.* (1995) demonstrated that a distinction can be made between bubbling and non-bubbling systems through transient integration of the above system of equations, coupled with the following simple, physically credible closures:

$$\boldsymbol{f} = (1-\phi)\,\beta(\boldsymbol{u}-\boldsymbol{v}), \tag{5}$$

$$\boldsymbol{\sigma}_s = p_s \boldsymbol{I} - \mu_s[\boldsymbol{\nabla v} + (\boldsymbol{\nabla v})^T - \tfrac{2}{3}(\boldsymbol{\nabla}\cdot\boldsymbol{v})\boldsymbol{I}], \tag{6}$$

$$\boldsymbol{\sigma}_f = p_f \boldsymbol{I} - \hat{\mu}_f[\boldsymbol{\nabla u} + (\boldsymbol{\nabla u})^T - \tfrac{2}{3}(\boldsymbol{\nabla}\cdot\boldsymbol{u})\boldsymbol{I}]. \tag{7}$$

Equation (5) represents a drag force proportional to the local relative velocity and the factor β is deduced from the well-known Richardson–Zaki (1954) correlation to be

$$\beta = \frac{(\rho_s-\rho_f)\,g\phi}{v_t(1-\phi)^{n-1}}, \tag{8}$$

where n depends on the Reynolds number for an isolated particle falling at its terminal velocity, v_t. The effective viscosity of the fluid phase ($\hat{\mu}_f$) and pressure (p_f) are taken to be the viscosity of the pure fluid (μ_f) and local average value of the fluid pressure, respectively, while p_s and μ_s are assumed to be monotone increasing functions of ϕ which vanish when $\phi = 0$ and increase without bound as $\phi \to \phi_p$, where ϕ_p is the volume fraction of particles at random close packing. For the particle phase pressure and viscosity we adopt the same functional forms employed in ASJ and GKS1, namely,

$$p_s = C_1\,\phi^3 \exp\left[\frac{r\phi}{\phi_p-\phi}\right], \tag{9}$$

$$\mu_s = \frac{A\phi}{1-\left(\dfrac{\phi}{\phi_p}\right)^{1/3}}, \tag{10}$$

where C_1, r and A are positive constants, and are treated as model parameters. With the above closures, the equations of motion permit a solution representing a uniformly fluidized bed of infinite extent, with

$$\phi = \phi_0, \quad \boldsymbol{v} = \boldsymbol{0}, \quad \boldsymbol{u} = \boldsymbol{j}u_0,$$

$$\boldsymbol{\nabla} p = [\rho_s\phi_0 + \rho_f(1-\phi_0)]\,\boldsymbol{g}, \quad \beta u_0 = \phi_0(\rho_s-\rho_f)\,g,$$

where $\boldsymbol{j}$ is the unit vector in the y-direction pointing vertically upward, and ϕ_0 and u_0 are constants. It is well known that when the mean volume fraction of particles in the bed, ϕ_0, is smaller than some critical value, ϕ_c, the state of uniform fluidization is linearly unstable and the fastest growing disturbance is an upward travelling wave with no horizontal structure (Anderson & Jackson 1968). This one-dimensional travelling wave takes the form of alternating bands of high and low voidage, which move upward

through the bed, irrespective of whether the system is bubbling or not (ASJ). Two-dimensional travelling wave solutions are obtained through loss of stability of the 1D-TWs to transverse perturbations. Further discussion of these features can be found in ASJ and GKS1.

The sensitivity of the bifurcation structure to the assumed functional forms for p_s and μ_s has been examined by Glasser (1996). It is simply noted here that the key features of the solution structure, namely the birth of 1D-TWs from the uniform state through a Hopf bifurcation and the emergence of 2D-TWs from 1D-TWs, are insensitive to the assumed forms. This robustness has already been demonstrated in GKS1 through several examples. Thus, the qualitative features discussed in the present manuscript are not limited to the speculative closures given in (9) and (10).

2.1. *Relevant dimensionless groups and parameters*

Casting the model equations in a dimensionless form, using

$$\rho_s, v_t, L = \left(\frac{Av_t}{\rho_s g}\right)^{1/2}, \quad T = \frac{L}{v_t},$$

as characteristic density, velocity, length and time, respectively (GKS1), one obtains the following dimensionless groups:

$$\delta = \frac{\rho_f}{\rho_s}, \qquad \text{density ratio}$$

$$\gamma = \frac{\hat{\mu}_f}{A}, \qquad \text{viscosity ratio}$$

$$\alpha = \frac{C_1}{\rho_s v_t^2}, \quad \text{particle phase pressure coefficient}$$

$$\Omega = \left(\frac{\rho_s v_t^3}{Ag}\right)^{1/2}.$$

The model contains, in addition to these dimensionless groups, two other dimensionless parameters, namely, n and r.

Through a linear stability analysis of the state of uniform fluidization one can readily determine the value of ϕ_c as a function of the values of the model parameters: $\phi_c = \phi_c(\delta, \gamma, \alpha, \Omega, n, r)$ which can always be rewritten as $\alpha = \alpha(\delta, \gamma, \phi_c, \Omega, n, r)$. It has been argued in ASJ that the latter representation is more appropriate for the purpose of identifying the difference between bubbling and non-bubbling systems, and this has been adopted in GKS1 and the present study.

3. Numerical results

We will first present computational results for three specific systems which have been studied experimentally before. The dimensional and dimensionless parameters for these systems are listed in table 1. The 200 μm glass beads fluidized by ambient air (column 1) constitute a bubbling system, and its bifurcation behaviour has been

	Glass beads in air	Glass beads in water	Lead shot in water
ρ_s	2.2 g cm^{-3}	2.2 g cm^{-3}	11.3 g cm^{-3}
ρ_f	0.001 3 g cm^{-3}	1.0 g cm^{-3}	1.0 g cm^{-3}
μ_f	0.018 1 cP	1.0 cP	1.0 cP
a	100 μm	500 μm	500 μm
v_t	142 cm s^{-1}	14.3 cm s^{-1}	49.0 cm s^{-1}
ϕ_p	0.65	0.65	0.65
ϕ_c	0.576	0.576	0.576
ϕ_0	0.57	0.57	0.57
A	0.5 p	0.5 p	0.5 p
$\mu_s(\phi_0)$	6.65 p	6.65 p	6.65 p
C_1	1.08 Pa	0.026 53 Pa	2.135 Pa
r	0.3	0.3	0.3
L	0.182 cm	0.057 6 cm	0.047 0 cm
T	0.001 28 s	0.004 03 s	0.000 960 s
R_t	20	143	490
n	4.35	3.70	3.39
δ	0.000 591	0.455	0.088 5
γ	0.000 363	0.02	0.02
α	0.000 242	0.000 590	0.000 787
Ω	113.7	3.623	52.09
B	3.5	2.5	10.5

TABLE 1. Values of parameters and dimensionless groups for the fluidized beds. First column, 200 μm diameter glass beads in air; second column, 1 mm diameter glass beads in water; third column, 1 mm diameter lead shot in water.

presented in GKS1. The system of 1 mm glass beads fluidized by water (column 2) is known to be non-bubbling. We will consider the system of 1 mm lead shot fluidized by water (column 3) to be a bubbling system, as it has been observed that pockets of water injected into such a bed develop into bubbles which retain their integrity (Harrison, Davidson & de Kock 1961). Our goal is to examine whether the differences in behaviour can be captured if the same rheological assumptions are made for the various beds. We have therefore adopted the same closure relations for the different cases. It is known experimentally that these three systems start to exhibit time-dependent flow patterns at approximately the same volume fraction. With this in mind, the critical volume fraction, ϕ_c, has been assumed to be the same for all three systems. The parameters C_1 and r in (9) permit the magnitude and slope of the particle pressure, and hence ϕ_c, to be adjusted. We have taken r to be the same for the different cases. It then follows that the parameter C_1 in (9) will have to be different for the three systems (see table 1). The terminal settling velocities were calculated using the empirical correlations from Kunii & Levenspiel (1991). Much less is known about the appropriate choice of A for these systems. We will assign, for the time being, the same value of A for all three systems, and return to this issue later on. The volume fraction of particles in the uniform state, ϕ_0, has been set to be 0.57 in all three cases. As $\phi_0 < \phi_c$, this uniform state is unstable in all three cases. We will examine in detail the consequences of this instability. We simply note here that we have analysed a number of different fluidized bed systems and that the cases described in table 1 are representative examples. Subsequently, we will discuss results obtained for several different combinations of the dimensionless groups to bring forth the key parameter that separates bubbling and non-bubbling systems.

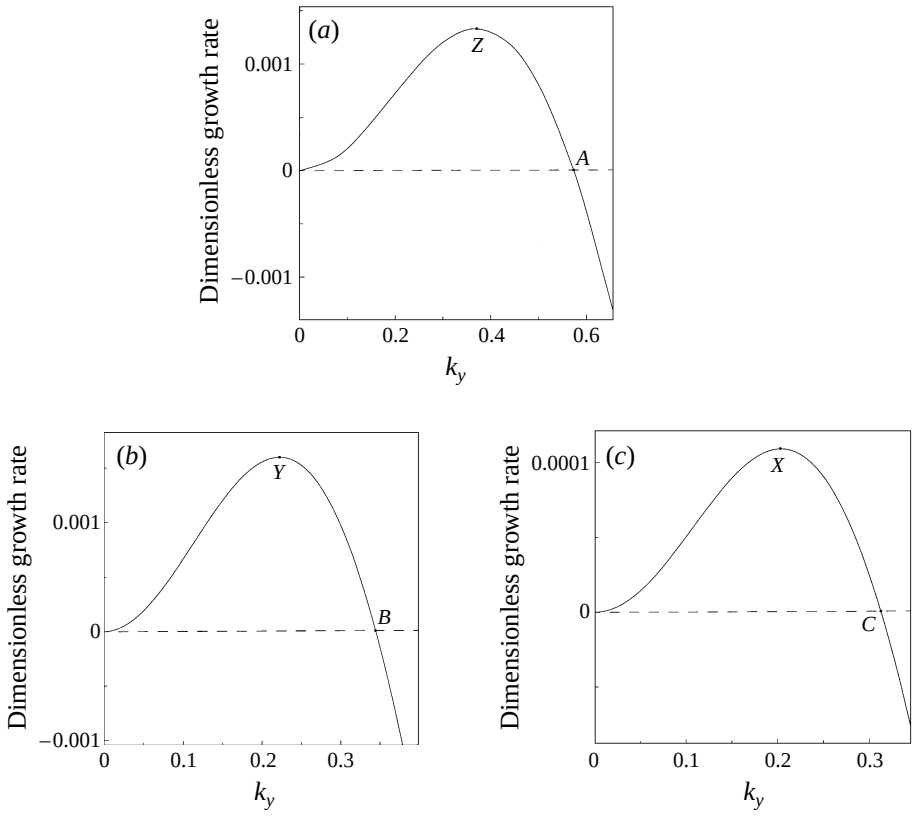

FIGURE 1. Linear stability of the uniform state for $k_x = 0$. Real part of the (complex) growth rate as a function of k_y, $\phi_0 = 0.57$. (*a*) Glass beads in air. (*b*) Lead shot in water. (*c*) Glass beads in water.

3.1. *Linear stability of the uniform state*

The linear stability of the uniform state, $\phi_0 = 0.57$, against small one-dimensional (vertical) disturbances is easily analysed. The results of this analysis for the three systems in table 1 are summarized in figure 1, where the real part of the complex growth rate of one-dimensional disturbances is plotted against their vertical wavenumber k_y (dimensionless). The horizontal wavenumber, k_x, is zero for all the curves. For all k_y values, the growth rate is complex, indicating that the instability is a travelling wave (not shown). The maximum growth rates for the glass beads in air (point Z) and lead shot in water (point Y) are comparable, while that for the case of glass beads in water (point X) is an order of magnitude smaller; this was noted by Jackson (1963) over three decades ago.

3.2. *One-dimensional travelling waves*

Points A, B and C in figure 1 correspond to the Hopf bifurcation points, each of which signals the birth of a family of one-dimensional travelling wave (1D-TW) solutions away from the uniform state. Every 1D-TW is characterized by two parameters, namely, ϕ_0 and k_y. We will be mostly concerned with the family of 1D-TWs generated by holding ϕ_0 constant and allowing k_y to vary. Each 1D-TW will have its own (dimensionless) wave speed with respect to the laboratory frame (defined as the frame of reference where the average flux of particles in the periodic box is zero), c, which is determined as a part of the solution. In a frame of reference moving at this wave speed, the wave will appear as a steady solution. The procedure to compute these 1D-TWs

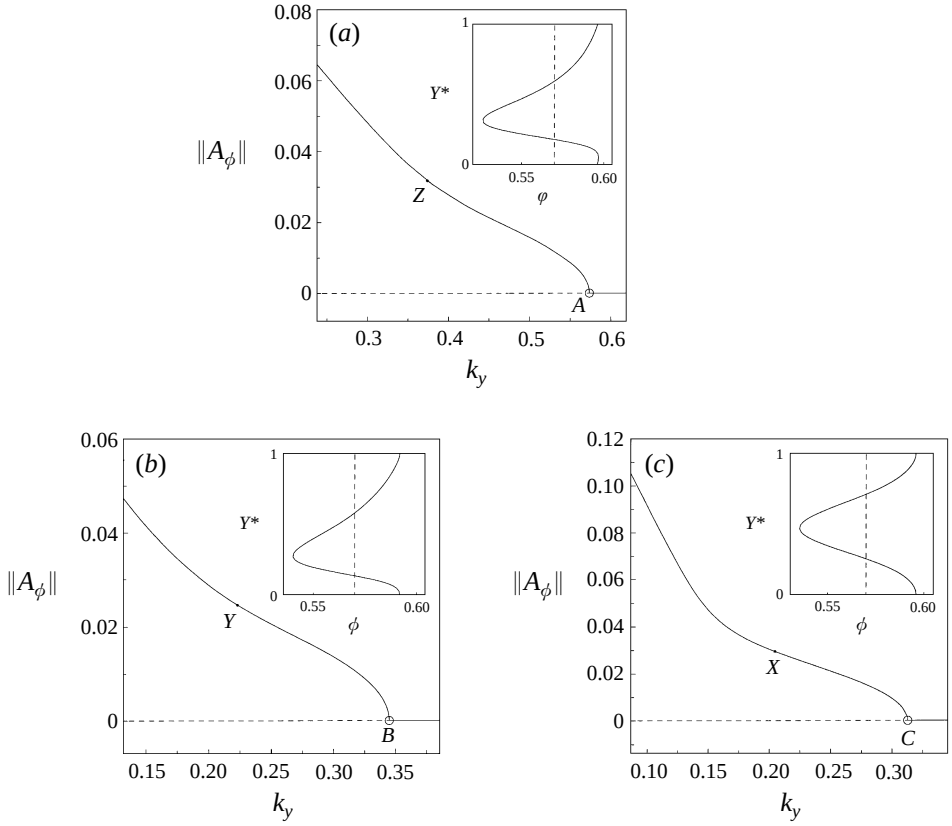

FIGURE 2. Bifurcation diagrams for one-dimensional travelling waves. Volume fraction of solids norm, $\|A_\phi\|$, versus k_y, $\phi_0 = 0.57$. (*a*) Glass beads in air. Inset is one-dimensional travelling wave corresponding to point *Z*. (*b*) Lead shot in water. Inset is one-dimensional travelling wave corresponding to point *Y*. (*c*) Glass beads in water. Inset is one-dimensional travelling wave corresponding to point *X*.

through a continuation scheme starting from the Hopf bifurcation point has been discussed in GKS1. In these calculations, all the dependent variables appearing in the model are approximated with a Fourier series in the wave frame. Figure 2 shows the particle volume fraction norm, $\|A_\phi\|$, as a function of k_y for the three fluidized beds described in table 1 (and figure 1). The average volume fraction of particles, ϕ_0, in each 1D-TW is 0.57. The volume fraction norm, $\|A_\phi\|$, is the L_2 norm of the Fourier coefficients for the particle volume fraction (GKS1). The mean volume fraction of particles in the wave is not included in the norm, so the base (uniform) state is represented by the line $\|A_\phi\| = 0$. Thus, $\|A_\phi\|$ gives a measure of the amplitude of the solution with respect to the uniform state. Points *X*, *Y* and *Z* in figure 2 correspond to their namesakes in figure 1. The 1D-TWs corresponding to these three points are shown as insets in figure 2. It is readily apparent that these waves are qualitatively similar, so bubbling and non-bubbling beds cannot be distinguished on the basis of the structure of 1D-TWs (Dankworth & Sundaresan 1991; ASJ).

3.3. *Stability of 1D-TWs to two-dimensional perturbations*

The linear stability of each of the three 1D-TWs in the insets of figure 2 against small disturbances which posses the same *y*-periodicity as the 1D-TW itself and are also

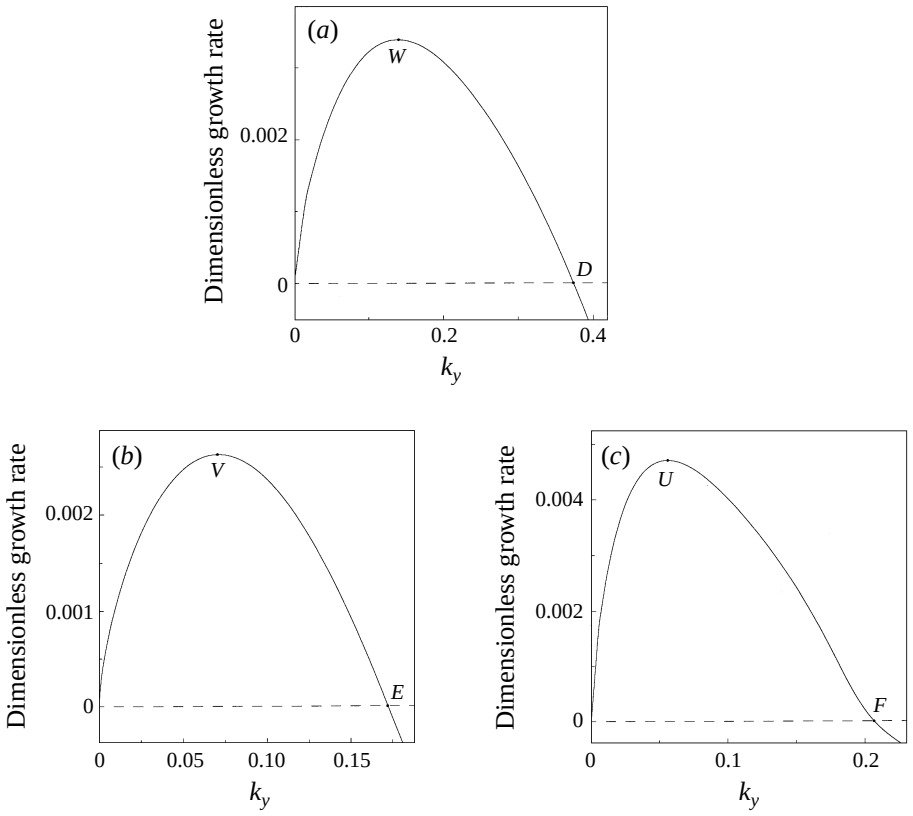

FIGURE 3. Linear stability of fully developed one-dimensional travelling wave for $\phi_0 = 0.57$. (*a*) Glass beads in air, $k_y = 0.373$. (*b*) Lead shot in water, $k_y = 0.223$. (*c*) Glass beads in water, $k_y = 0.204$.

periodic in the x-direction has been analysed, and the results are summarized in figures 3–6. The growth rate of the disturbance as a function of k_x is shown in figures 3(*a*)–3(*c*) for the three 1D-TWs corresponding to points Z, Y and X in figure 2, respectively. It can be seen that for all three cases the 1D-TW is stable for large k_x. As k_x is decreased one real eigenvalue goes through zero and becomes positive (when the 1D-TW is viewed from a frame of reference moving with the wave). The points at which the eigenvalue goes through zero (marked as points D, E and F in figures 3(*a*)–3(*c*) signal the birth of two-dimensional travelling wave solutions. Note that the maximum growth rates for the two-dimensional instability for these three 1D-TWs (points U, V and W) are comparable in magnitude. This is in sharp contrast with the growth rates for the one-dimensional instability away from the uniform state (see figure 1*a–c*). This difference has been noted previously by ASJ.

The eigenfunction corresponding to the most unstable eigenvalue leading to the instability of the 1D-TW for the 'lead shot in water' system (point V in figure 3*b*) is presented in figure 4. The spatial variation of ϕ in the 1D-TW is shown in figure 4(*a*). The eigenfunctions associated with particle volume fraction, fluid phase velocity and particle phase velocity are shown in figures 4(*b*), 4(*c*) and 4(d), respectively. The quantities N and M in the figure caption refer to the number of Fourier modes in the y- and x-directions, respectively, used to generate the results shown in the figure. Each of these figures displays spatial variation over one periodic cell of height $2\pi/k_y$ and width $2\pi/k_x$. The eigenfunctions corresponding to point U in figure 3(*c*) (for the 'glass

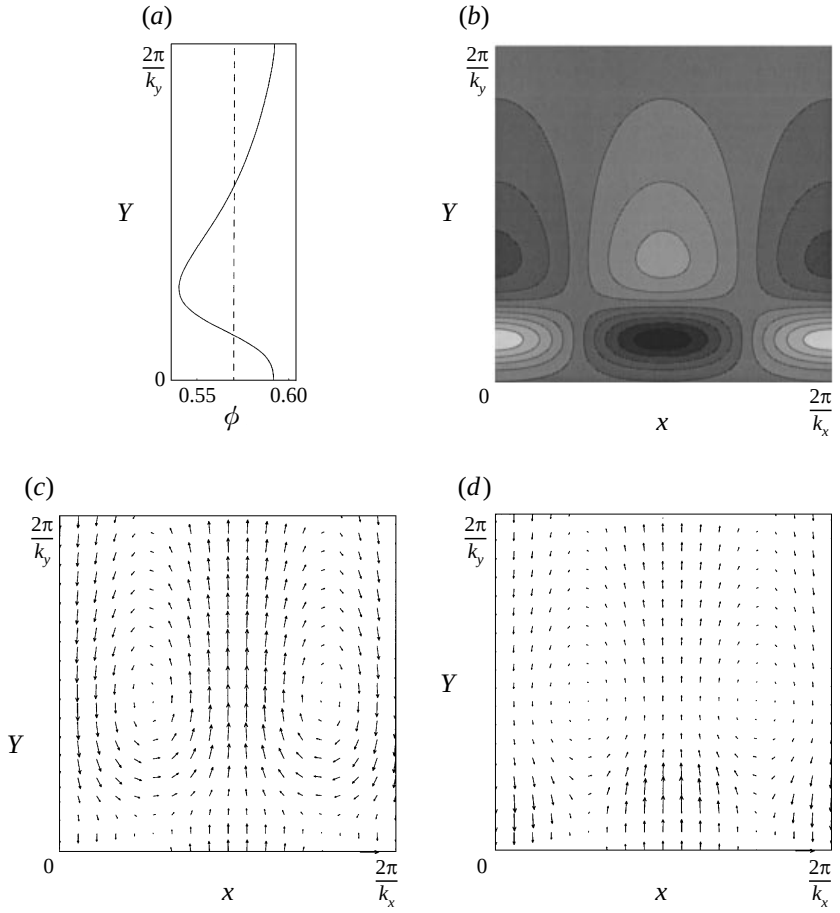

FIGURE 4. Eigenfunctions corresponding to maximum growth rate (point V) in figure 3(b). Lead shot in water; $k_y = 0.223$, $k_x = 0.0700$, $N = 4$, $M = 1$. (a) The corresponding one-dimensional travelling wave, height versus volume fraction of solids. The broken line shows the mean volume fraction of solids, $\phi_0 = 0.57$. (b) Grey-scale plot of the eigenfunction corresponding to the volume fraction of solids. The increments between shades of grey are equal. (c) Vector plot of fluid velocity eigenfunction. (d) Vector plot of solids velocity eigenfunction. Although the eigenfunctions are shown in a square box, the actual periodic box has unequal k_x and k_y.

beads in water' system) are shown in figure 5. A similar figure for the 'glass beads in air' system can be found in GKS1 (figure 7). It is clear from these figures that the eigenfunctions for all three cases are qualitatively similar. The quantitative differences can be accounted for by the different amplitudes of the 1D-TWs and different extents of asymmetry in these waves. In general, the extent of asymmetry in a 1D-TW increases as its amplitude increases. The 1D-TW for the case of glass beads in water shown in figure 5(a) is much less asymmetric than the waves for the other two cases. Higher-amplitude 1D-TWs in the glass beads in water case do indeed develop appreciable asymmetry (ASJ; Glasser 1996). However, when waves of the same amplitude are compared, then the 1D-TW corresponding to glass beads in water does not have the same degree of asymmetry as the 1D-TWs in the other two beds.

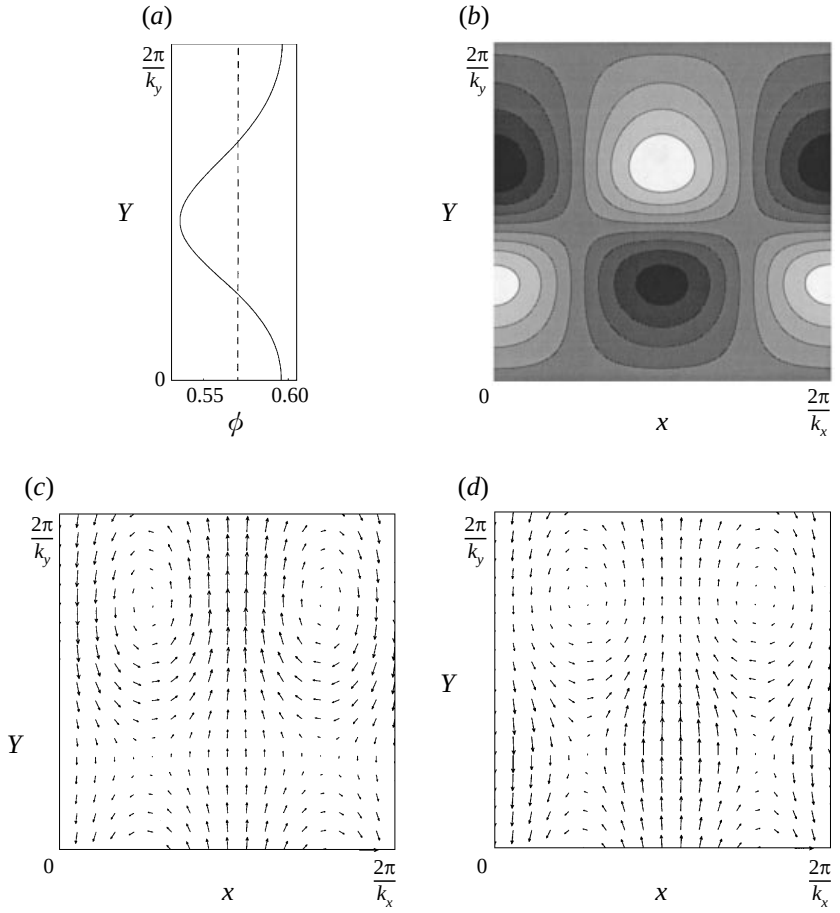

FIGURE 5. Eigenfunctions corresponding to maximum growth rate (point U) in figure 3(c). Glass beads in water, $k_y = 0.204$, $k_x = 0.0634$; $N = 4$, $M = 1$. See figure 4 for description.

3.4. *Two-dimensional travelling waves*

Every fully-developed 2D-TW is characterized by three parameters, namely, ϕ_0, k_y and k_x. Each wave will have its own wave speed, c, which is determined as a part of the solution, as in the case of 1D-TWs. In a frame of reference moving at this wave speed, the wave will appear as a steady solution. We have computed these 2D-TWs through a continuation scheme starting from the point where these waves bifurcate from the 1D-TW (GKS1). In these calculations, all the dependent variables are approximated with a Fourier series in the wave frame, as in the case of 1D-TWs. The particle volume fraction norm, $\|A_\phi\|$, is again the L_2 norm of the Fourier coefficients for ϕ, ignoring the average volume fraction, ϕ_0. Further details of the computational scheme can be found elsewhere (GKS1; Glasser 1996).

Figures 6(a)–6(c) show $\|A_\phi\|$ as a function of k_y for the three representative fluidized beds. These figures include both the uniform state and the families of 1D-TWs and 2D-TWs. The average volume fraction of particles in every solution contained in these figures is 0.57. We have also set $k_x = k_y$. (Figure 6(a) has been presented in our earlier paper, GKS1, as figure 10. It is repeated here for the sake of completeness.) The uniform state, represented by $\|A_\phi\| = 0$, loses stability at the Hopf bifurcation point (A, B and C in figures 6(a), 6(b) and 6(c), respectively). Solutions on the 1D-TW

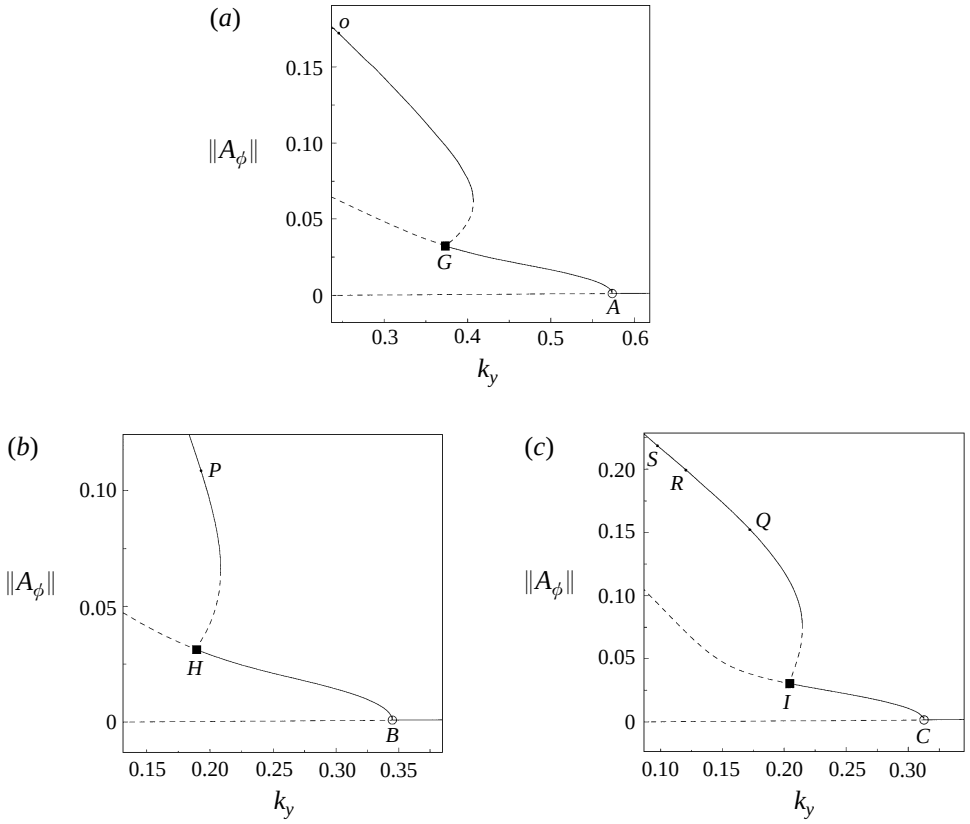

FIGURE 6. Bifurcation diagrams showing the uniform state and one- and two-dimensional travelling wave solutions. $k_x = k_y$. ——, stable branches; ---, unstable branches. (*a*) Glass beads in air. (*b*) Lead shot in water. (*c*) Glass beads in water.

branch emerging from this point increase in amplitude and extent of asymmetry as one moves away from the Hopf bifurcation point. In all three cases shown, the 2D-TW branch bifurcates from the 1D-TW branch in a subcritical fashion at points *G*, *H* and *I* in figures 6(*a*), 6(*b*) and 6(*c*), respectively. This branch subsequently turns around and gains stability. It is important to spell out what is meant by stability in the present context. Two-dimensional travelling waves shown in these figures as solid curves are stable to small two-dimensional disturbances which retain the same periodicity as the wave itself, and have *x*- and *y*-wave harmonics larger than or equal to the *x*- and *y*-wavenumbers of the wave, respectively. The segments shown by dashed lines in these figures are unstable to such disturbances. Note that high-amplitude 2D-TWs, which are linearly stable, are possible for both bubbling and non-bubbling systems, i.e. if they formed somehow, they would remain. It is readily apparent that, within the framework of the assumed mathematical model, all three fluidized beds manifest an identical hierarchy of bifurcations, demonstrating very clearly that bubbling and non-bubbling beds cannot be distinguished on this basis.

Solutions at various points on the 2D-TW branch (for the case of 200 μm glass beads fluidized by air) in figure 6(*a*) have been discussed in detail in GKS1. We simply note here that the two-dimensional structure becomes increasingly pronounced as we move away from the bifurcation point (point *G* in figure 6*a*) and that a bubble-like hole can be readily seen in high-amplitude 2D-TWs. This is illustrated in figure 7, where the 2D-

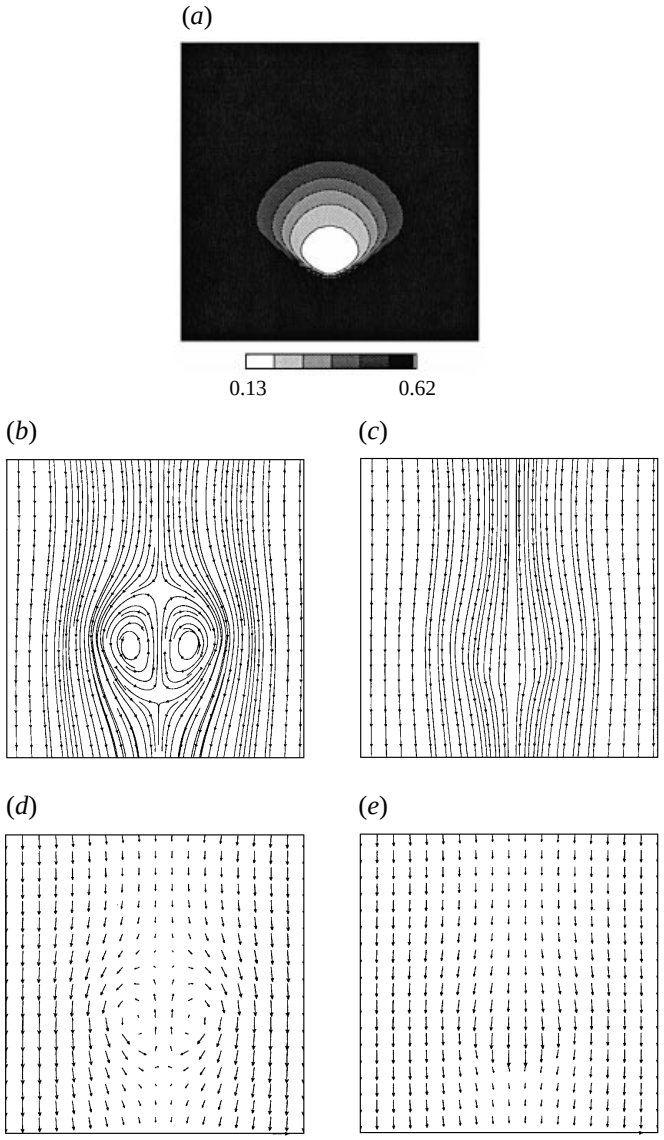

FIGURE 7. Two-dimensional travelling wave solution, corresponding to point O in figure 6(*a*). $k_x = k_y = 0.246$, $N = 36$, $M = 24$, $c = 0.155$. (*a*) Volume fraction of solids. (*b*) Streamline plot of fluid velocity. (*c*) Streamline plot of solids velocity. (*d*) Vector plot of fluid velocity (longest vector = $0.160v_t$). (*e*) Vector plot of solids velocity (longest vector = $0.247v_t$). *Note*: all streamlines in this figure and later figures should connect. Those streamlines that suggest spirals or disconnected segments are artifacts of our plotting routine.

TW solution at point O in figure 6(*a*) is presented. The plots in this figure and all subsequent figures showing fully developed travelling waves are presented in a frame of reference moving with the wave. The presence of a bubble-like hole in the ϕ-structure (figure 7*a*), a recirculation pattern in the gas streamlines inside the hole (figure 7*b*) and a slight bending of the particle phase streamlines around the hole (figure 7*c*) are clearly evident. The fluid and particle phase velocities at various locations in the periodic box, measured from a frame of reference moving with the wave, are shown in figures 7(*d*) and 7(*e*). The largest speed attained by the fluid phase (recorded as the

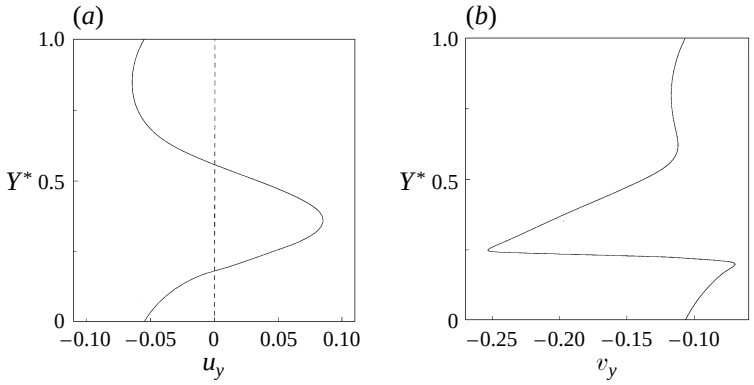

FIGURE 8. Fluid and solids velocities along the vertical centreline (the axis of symmetry of the solution) in figure 7. Velocity versus scaled height, Y^*. (*a*) Fluid velocity. (*b*) Solids velocity. The velocities are measured with respect to the wave frame.

longest vector in figure 7(*d*) is clearly in the dense phase region surrounding the central hole. In contrast, the highest speed attained by the particle phase is inside the hole (figure 7*e*). The vertical components of these velocities at various points along the vertical centreline of the cell (which is the axis of symmetry of the solution) are plotted in figures 8(*a*) and 8(*b*), respectively. The dimensionless wave speed, c, for the 2D-TW shown in figures 7 and 8 is 0.155. The fluid attains its largest upward velocity inside the bubble-like hole. The magnitude of this velocity is about 0.08 v_t, which is roughly half the wave velocity (figure 8*a*). The particles accelerate as they enter the bubble-like hole through its roof, and then decelerate as they exit the bubble (figure 8*b*).

The manner in which the solution structure evolves along the 2D-TW branch for the case of 1 mm lead shot fluidized by water (figure 6*b*) is very similar to that observed for the case of 200 μm glass beads fluidized by air. The 2D-TW solution at point P in figure 6(*b*) is presented in figure 9. The corresponding vertical velocities along the vertical centreline are shown in figure 10. The similarity between figures 7 and 9, and figures 8 and 10 is striking. As in the previous case, the particles move down through the hole (in the wave frame), accelerating at first and then decelerating. The largest speed attained by the fluid is in the particle-rich region surrounding the central hole, while the largest speed attained by the particle phase is inside the hole. The largest upward velocity attained by the fluid inside the hole is about 0.12 v_t, which is again roughly half the wave velocity (figure 10*a*).

We have examined a number of fully-developed 2D-TW solutions, which have smaller k_y ($= k_x$) values than those shown in figures 7 (for the glass beads in air system) and 9 (for the system of lead shot in water). As k_y decreases, the volume fraction norm increases, and the particle concentration in the hole decreases. Nevertheless, the qualitative features of the travelling wave solutions remain unaltered.

The evolution of fully developed solution structure along the 2D-TW branch for the case of 1 mm glass beads fluidized by water (figure 6*c*) differs from those for the cases of lead shot in water and glass beads in air in subtle ways that are not captured by projections of the type shown in figure 6. In order to describe these differences, let us examine the solutions at two points, Q and S, on the 2D-TW branch in figure 6(*c*). The 2D-TW solution at point Q, shown in figure 11, consisting of a central hole with a low concentration of particles, a recirculation of fluid in this high voidage region and a bending of particle phase streamlines around the hole, is qualitatively similar to those presented earlier in figures 7 and 9 for the cases of glass beads in air and lead shot in

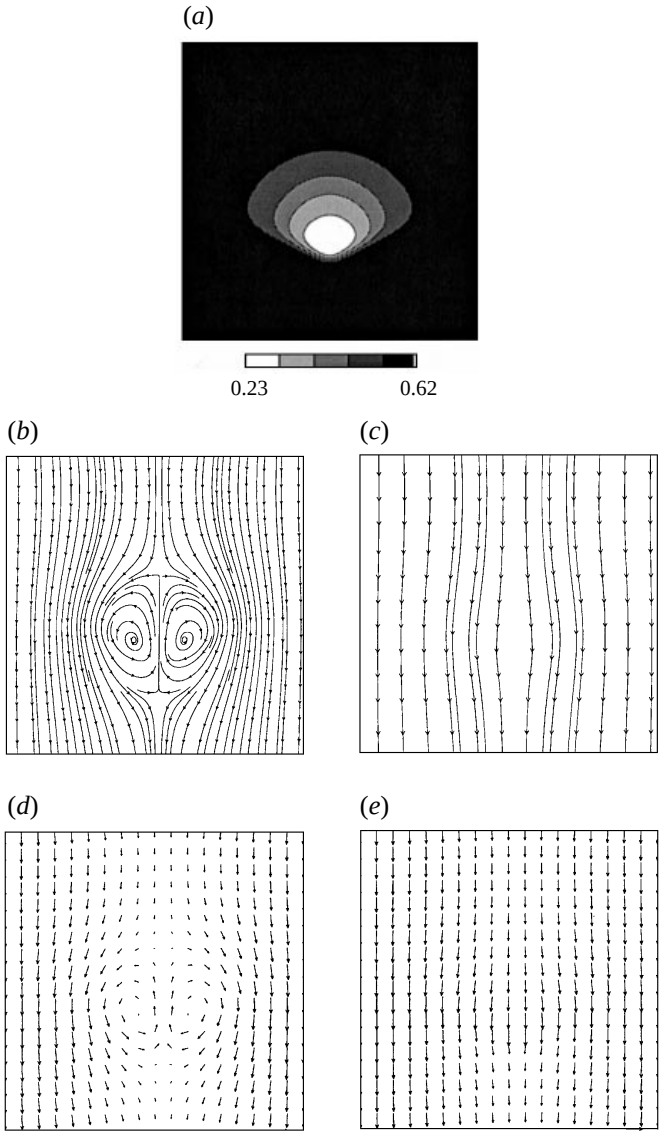

FIGURE 9. Two-dimensional travelling wave solution, corresponding to point P in figure 6(*b*). $k_x = k_y = 0.188$, $N = 24$, $M = 12$, $c = 0.238$. (*a*) Volume fraction of solids. (*b*) Streamline plot of fluid velocity. (*c*) Streamline plot of solids velocity. (*d*) Vector plot of fluid velocity (longest vector = $0.181 v_t$). (*e*) Vector plot of solids velocity (longest vector = $0.295 v_t$).

water. The y-components of the fluid and particle phase velocities along the vertical centreline, shown in figure 12, resemble those shown earlier in figures 8 and 10. As in the other two cases, the particles move down through the bubble-like hole, accelerating first and then decelerating (figure 12*b*). The largest upward fluid velocity attained in the hole is about 0.2 v_t, which is roughly 75% of the wave velocity (figure 12*a*). This is larger than the ratio of 0.5 recorded in the other two cases, so a quantitative difference can be noted. Also, the shape of the hole in figure 11(*a*) is noticeably different from those seen earlier in figures 7(*a*) and 9(*a*). The highest speed attained by the fluid phase is in the particle-rich region surrounding the hole (figure 11*d*), as in the previous two

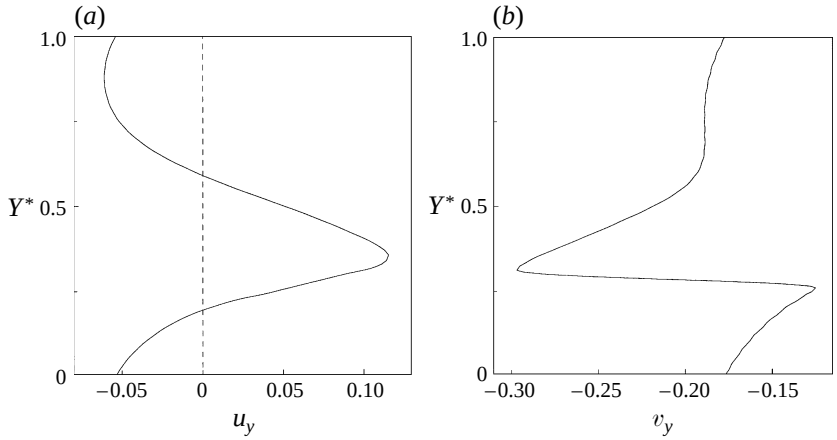

FIGURE 10. Fluid and solids velocities along the vertical centreline (the axis of symmetry of the solution) in figure 9. Velocity versus scaled height, Y^*. (*a*) Fluid velocity. (*b*) Solids velocity. The velocities are measured with respect to the wave frame.

cases. The longest velocity vector for the particle phase (0.367 v_t) is also located in the particle-rich region (see figure 11*e*). This was not the case in the two cases described earlier. This, however, is not a dramatic difference as the highest speed reached by the particle phase inside the hole is only slightly smaller than in the previous figures.

The 2D-TW associated with point S in figure 6(*c*) is shown in figure 13 and the corresponding centreline velocities are presented in figure 14. This solution has a larger volume fraction norm than that corresponding to point Q (see figure 6*c*). The volume fraction of particles in the central hole of figure 13(*a*) is significantly smaller than that in the hole shown in figure 11(*a*). The velocity vectors presented in figures 13(*d*) and 13(*e*), and the centreline velocities shown in figure 14 do reveal a dramatic difference between this 2D-TW and the ones presented earlier. The longest velocity vector for the fluid phase (in the wave frame) is now associated with the upward flow of fluid inside the hole, which is in sharp contrast with the previous cases. The largest upward fluid velocity attained in the hole exceeds v_t, and is well above the wave velocity with respect to the laboratory frame. A consequence of this rapid upflow of fluid in the hole is the significant alteration of the velocity field of the particles inside the hole. The particles still enter the bubble-like hole through the roof and they accelerate initially. However, as they move down through the hole, they quickly decelerate upon encountering the fluid rising rapidly upwards through the hole. This is followed by a rapid acceleration in the region where the upward velocity of the fluid is beginning to decrease, and a final deceleration as the particles exit the hole. During the intermediate deceleration, the downward velocity of the particles (in the wave frame) dips down to about 0.05 v_t. This feature of intermediate deceleration of particles inside the bubble-like hole is present in the solution corresponding to point R in figure 6(*c*) as well, where the smallest downward velocity attained by the particle phase during the intermediate deceleration (in the wave frame) is 0.28 v_t. As k_y ($= k_x$) is further decreased past point S (in figure 6*c*), the amplitude of the 2D-TW solution continues to increase and the volume fraction of particles in the hole continues to decrease; the smallest downward velocity attained by the particles during the intermediate deceleration inside the hole continues to decrease; we searched, but did not find any case where the particle velocity changes sign, indicating an upflow of particles inside the hole. It is also interesting to note that, in the solution corresponding to point S, the longest velocity vector for the particle

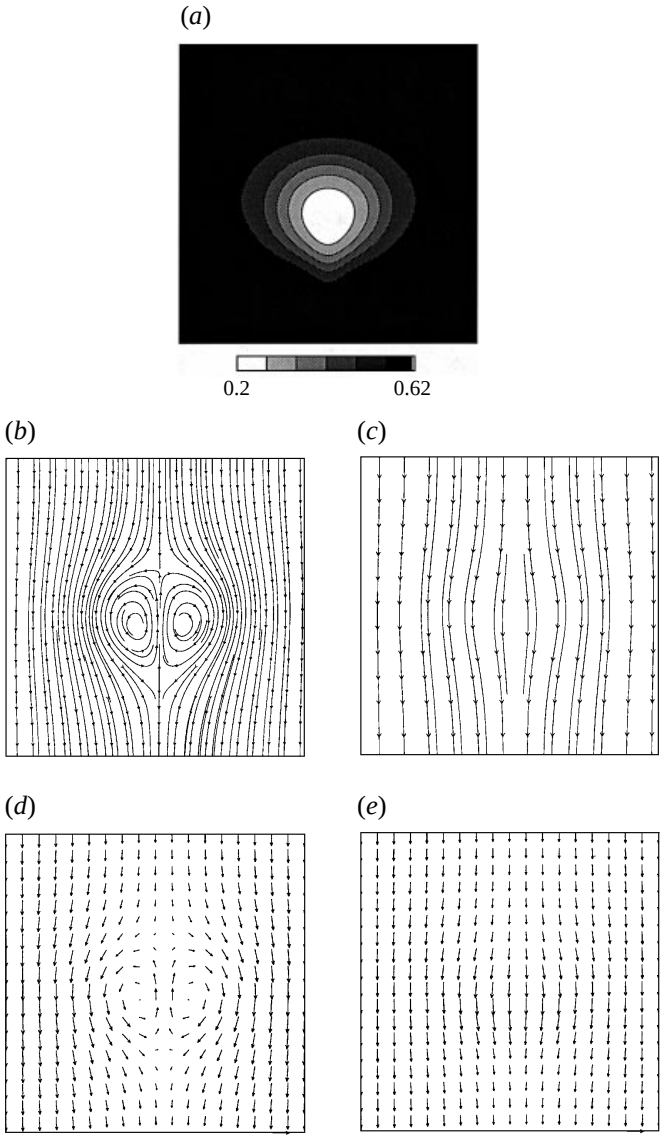

FIGURE 11. Two dimensional travelling wave solution, corresponding to point Q in figure 6(c). $k_x = k_y = 0.173$, $N = 18$, $M = 13$, $c = 0.262$. (a) Volume fraction of solids. (b) Streamline plot of fluid velocity. (c) Streamline plot of solids velocity. (d) Vector plot of fluid velocity (longest vector = $0.235v_t$). (e) Vector plot of solids velocity (longest vector = $0.367v_t$).

phase is located in the particle-rich region surrounding the hole, and has a magnitude of 0.845 v_t, which is significantly larger than the highest speed achieved by the particles inside the hole.

In the bifurcation analysis presented above, we have assumed that $k_y = k_x$. In order to ascertain that the features reported above are not restricted to square boxes, we repeated the analysis by holding both ϕ_0 and k_x constant, and treating k_y as the bifurcation parameter (Glasser 1996). Such bifurcation diagrams for the case of glass beads fluidized by air have been presented in GKS1, where it was found that, depending on the assumed value of k_x, the 2D-TW branch may emerge subcritically or

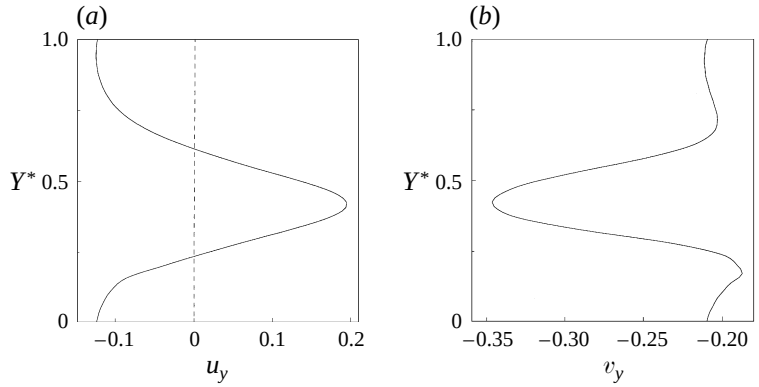

FIGURE 12. Fluid and solids velocities along the vertical centreline (the axis of symmetry of the solution) in figure 11. Velocity versus scaled height, Y^*. (*a*) Fluid velocity. (*b*) Solids velocity. The velocities are measured with respect to the wave frame.

supercritically from the 1D-TW branch. We simply note here that the same has been found to be true for all the systems (including those listed in table 1) analysed by us. However, the generic features of the bifurcation diagram, namely, the bifurcation of 1D-TWs from the uniform state and 2D-TWs from the 1D-TWs, always remained unaltered. In every case, large-amplitude 2D-TWs have bubble-like structures (Glasser 1996). Given the speculative nature of the closure relations for the stresses, we examined the sensitivity of the bifurcation structure to changes in the expressions used for particle phase pressure and viscosity (Glasser 1996). A detailed discussion of such a sensitivity analysis for the case of glass beads in air has been presented in GKS1. Again, we simply note that the generic features of the bifurcation diagram are robust and remain unaltered by these changes (Glasser 1996).

3.5. *Mathematical preliminaries for transient simulations*

We have now established the robustness of the basic bifurcation hierarchy and the persistence of the differences between high-amplitude solutions of non-bubbling (1 mm glass beads fluidized by water) and bubbling (200 μm glass beads fluidized by air and 1 mm lead shot fluidized by water) systems. It is, of course, hardly obvious why this difference should be adequate to distinguish *a priori* between bubbling and non-bubbling systems, as both systems manifest bubble-like holes which are linearly stable. Although we have been unable to prove this formally, we have been able to verify through transient integration of the averaged equations of motion that this difference is indeed significant. It will be shown below that fully developed 2D-TW solutions of the type shown in figures 7, 9 and 11, in which the particles enter the hole through the roof, accelerate only once and then decelerate as they exit the floor of the hole, readily evolve when the uniform state or the fully developed 1D-TW is subjected to a small two-dimensional perturbation. In contrast, fully developed solution structures such as that shown in figure 13, in which the particles travelling along the centreline of the hole experience additional deceleration and acceleration steps, do not develop even after a long period of integration; they are not accessible from the initial conditions resulting from small perturbations of the unstable uniform state.

The PDEs (namely, the averaged equations of motion) were transformed into a system of ODEs with algebraic constraints, through a spectral approximation of all the dependent variables (GKS1; Glasser 1996). The resulting system of differential and algebraic equations was then integrated using the routine DASSL (Petzold 1982). This

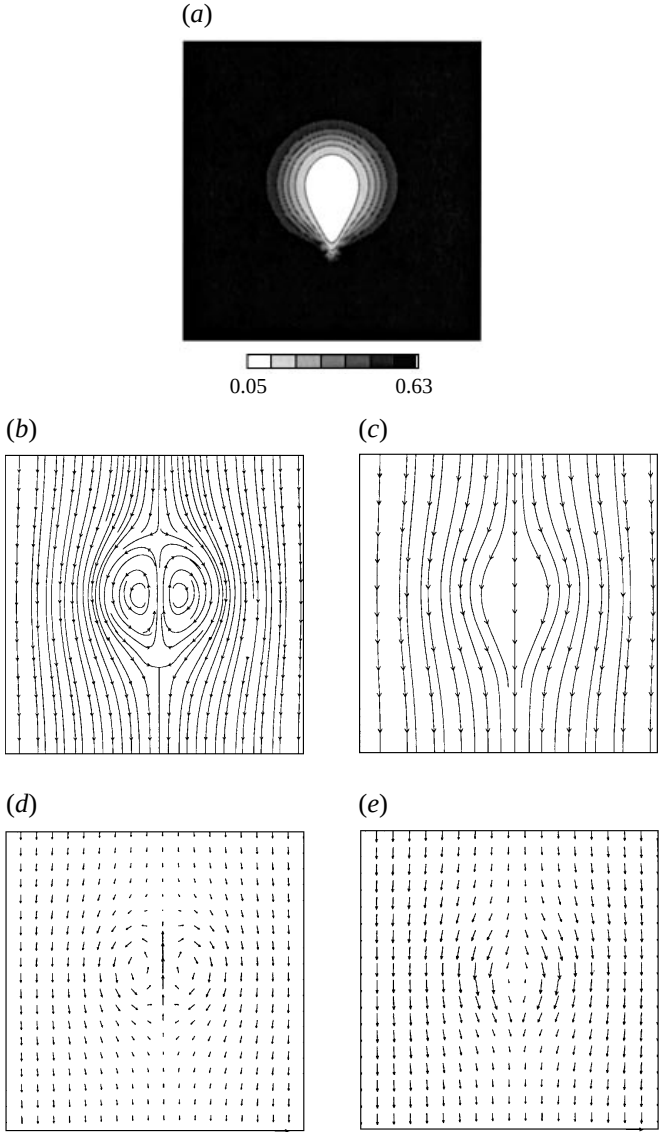

FIGURE 13. Two-dimensional travelling wave solution, corresponding to point S in figure 6(*c*). $k_x = k_y = 0.0979$, $N = 36$, $M = 24$, $c = 0.520$. (*a*) Volume fraction of solids. (*b*) Streamline plot of fluid velocity. (*c*) Streamline plot of solids velocity. (*d*) Vector plot of fluid velocity (longest vector = $1.06v_t$). (*e*) Vector plot of solids velocity (longest vector = $0.845v_t$).

code makes use of backward difference formulae of orders one to five to approximate the time derivative, and is based on the techniques introduced by Gear (1971). The results of the linear stability and bifurcation analyses can be used to test and validate transient integrations for accuracy and convergence. More traditional tests, consisting of variations in the size of the system (the number of Fourier modes, N and M, controlling the spatial discretization error), dealiasing, as well as variations of the local time-discretization error tolerance, were also performed to validate the computations presented here. We have generated our transients with different values of N and M, and checked that the same spatial structures were consistently obtained at the same times.

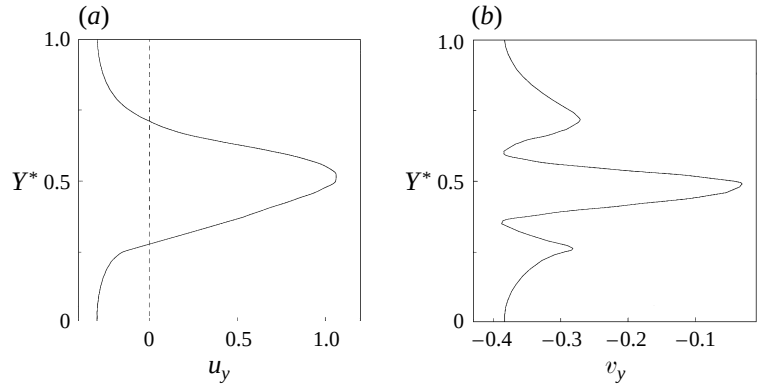

FIGURE 14. Fluid and solids velocities along the vertical centreline (the axis of symmetry of the solution) in figure 13. Velocity versus scaled height, Y^*. (*a*) Fluid velocity. (*b*) Solids velocity. The velocities are measured with respect to the wave frame.

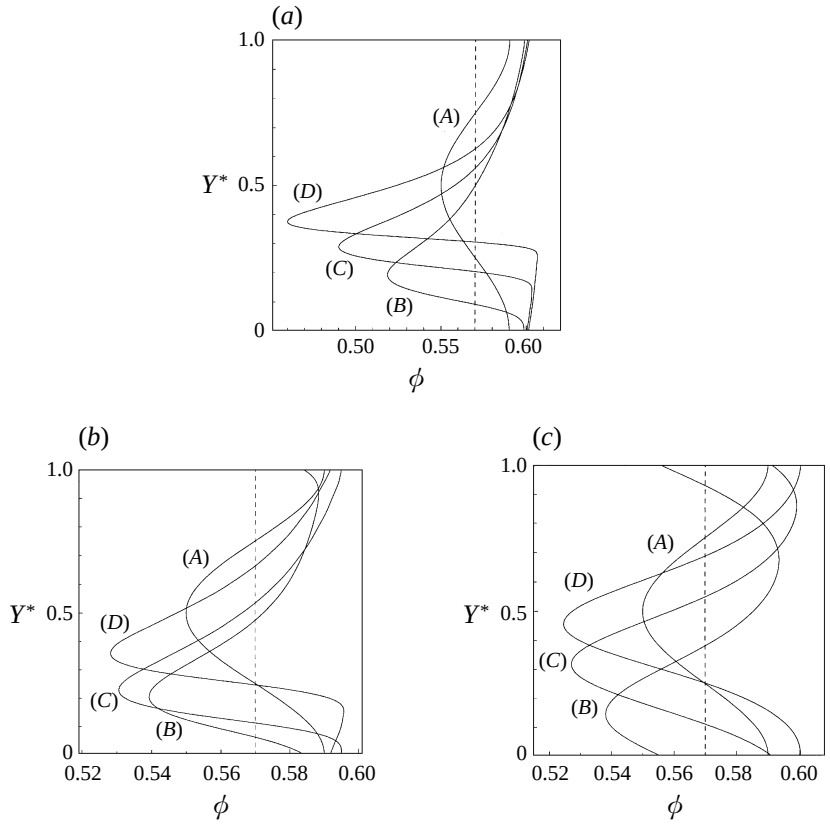

FIGURE 15. Development of 1D-TWs. (*a*) Glass beads in air, $k_y = 0.246$. (*A*) $\hat{t} = 0$, (*B*) $\hat{t} = 414$ ($t = 0.53$ s), (*C*) $\hat{t} = 797$ ($t = 1.02$ s), (*D*) $\hat{t} = 1508$ ($t = 1.93$ s). Initial wave speed, $c = 0.139$. Final wave speed, $c = 0.127$, $N = 15$. (*b*) Lead shot in water. $k_y = 0.188$. (*A*) $\hat{t} = 0$, (*B*) $\hat{t} = 104$ ($t = 0.1$ s), (*C*) $\hat{t} = 938$ ($t = 0.9$ s), (*D*) $\hat{t} = 2708$ ($t = 2.6$ s). Initial wave speed, $c = 0.238$. Final wave speed, $c = 0.227$, $N = 9$. (*c*) Glass beads in water, $k_y = 0.173$. (*A*) $\hat{t} = 0$, (*B*) $\hat{t} = 4715$ ($t = 19.0$ s), (*C*) $\hat{t} = 12159$ ($t = 49.0$ s), (*D*) $\hat{t} = 15137$ ($t = 61.0$ s). Initial wave speed, $c = 0.201$. Final wave speed, $c = 0.200$, $N = 9$.

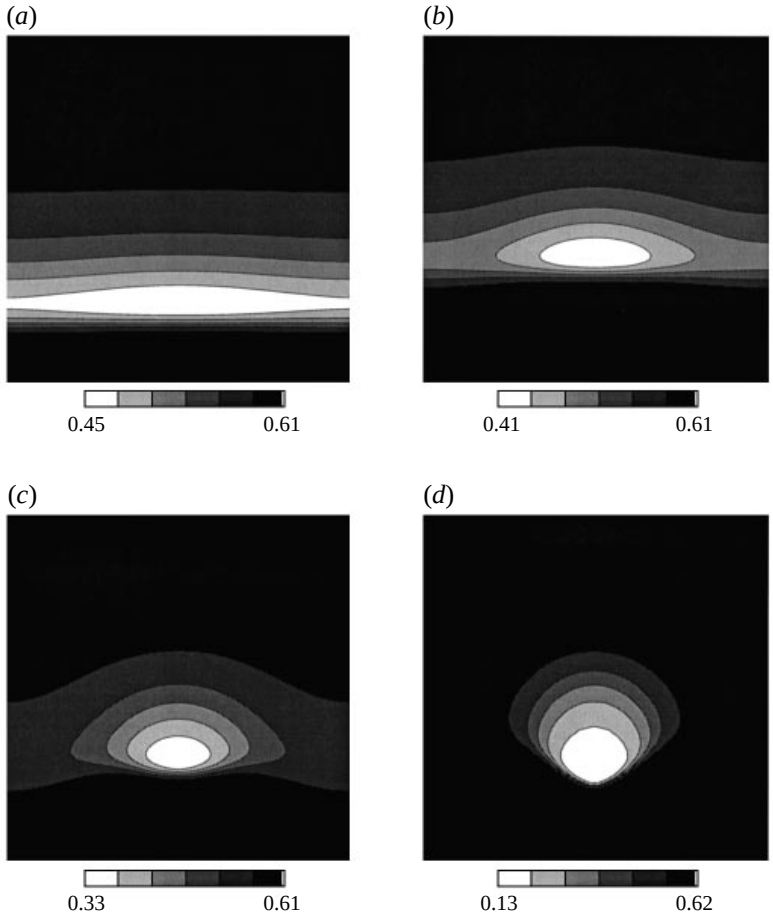

FIGURE 16. Growth of a perturbation of the 1D-TW for the air fluidized bed. $k_x = k_y = 0.246$. (*a*) $\hat{t} = 0$, $c = 0.127$. (*b*) $\hat{t} = 234$ ($t = 0.30$ s), $c = 0.129$. (*c*) $\hat{t} = 391$ ($t = 0.50$ s), $c = 0.135$. (*d*) $\hat{t} = 742$ ($t = 0.95$ s), $c = 0.155$. $N = 36$, $M = 24$.

Further details of our particular implementation can be found elsewhere (Glasser 1996).

3.6. *Evolution of 1D-TW structure from an unstable uniform state*

Our strategy for studying the transient development of large-amplitude nonlinear solutions consists of starting in the neighbourhood of the basic, unstable (saddle-type) solution and constructing initial conditions by adding (small) perturbations in the direction of the unstable modes. We therefore approximate solutions on the unstable manifold of the basic unstable state. More specifically, through a linear stability analysis of the uniform state, the most unstable one-dimensional eigenvalue (for the desired value of k_y) and the corresponding eigenfunction were determined. This eigenfunction was then scaled so that the maximum amplitude of the ϕ-perturbation was 0.02, and was added to the base state to construct the initial condition for the transient simulations. The evolution of one-dimensional ϕ-structures for glass beads in air, lead shot in water and glass beads in water are illustrated in figures 15(*a*)–15(*c*), respectively. The initial perturbation is sinusoidal in all three cases, and asymmetry develops as the wave moves through the bed. The timestep for numerical integration can be increased appreciably without sacrificing accuracy by following the evolution of

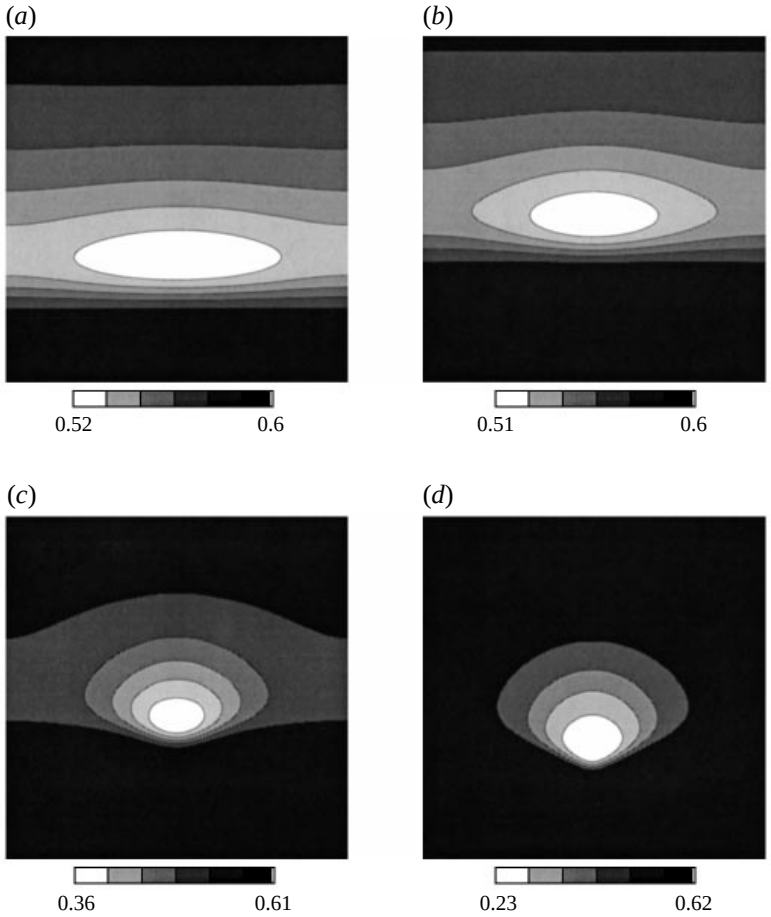

FIGURE 17. Growth of a perturbation of the 1D-TW for lead shot in water. $k_x = k_y = 0.188$. (*a*) $\hat{t} = 0$, $c = 0.227$. (*b*) $\hat{t} = 4688$ ($t = 4.5$ s), $c = 0.228$. (*c*) $\hat{t} = 7812$ ($t = 7.5$ s), $c = 0.230$. (*d*) $\hat{t} = 9479$ ($t = 9.1$ s), $c = 0.238$, $N = 24$, $M = 12$.

the wave from a frame of reference moving with an adaptive velocity close to the apparent velocity of the transient wave itself (ASJ). This procedure was adopted in the present study as well, so the relative positions of the ϕ-profiles shown in figures 15(*a*)–15(*c*) are arbitrary. The number of Fourier modes, N, reported in the captions of these figures is the minimum value needed to represent the solutions accurately (Glasser 1996). The figure captions include both dimensionless times ($\hat{t}$) and dimensional times (t). The order-of-magnitude growth times and the distance travelled by the waves during this growth process for the two bubbling systems are comparable (in both dimensional and dimensionless scales). However, as discussed by ASJ, the ϕ-structure in the non-bubbling system develops much more slowly and the wave travels a longer distance during the growth process.

3.7. *Evolution of 2D-TW structure from an unstable 1D-TW solution*

In the same spirit as above, an initial condition on the (one-dimensional) unstable manifold of the saddle-type unstable 1D-TW solution was constructed. Through a linear stability analysis of the 1D-TW, the most unstable eigenvalue (for the desired value of k_x) and the corresponding eigenfunction were determined. This eigenfunction

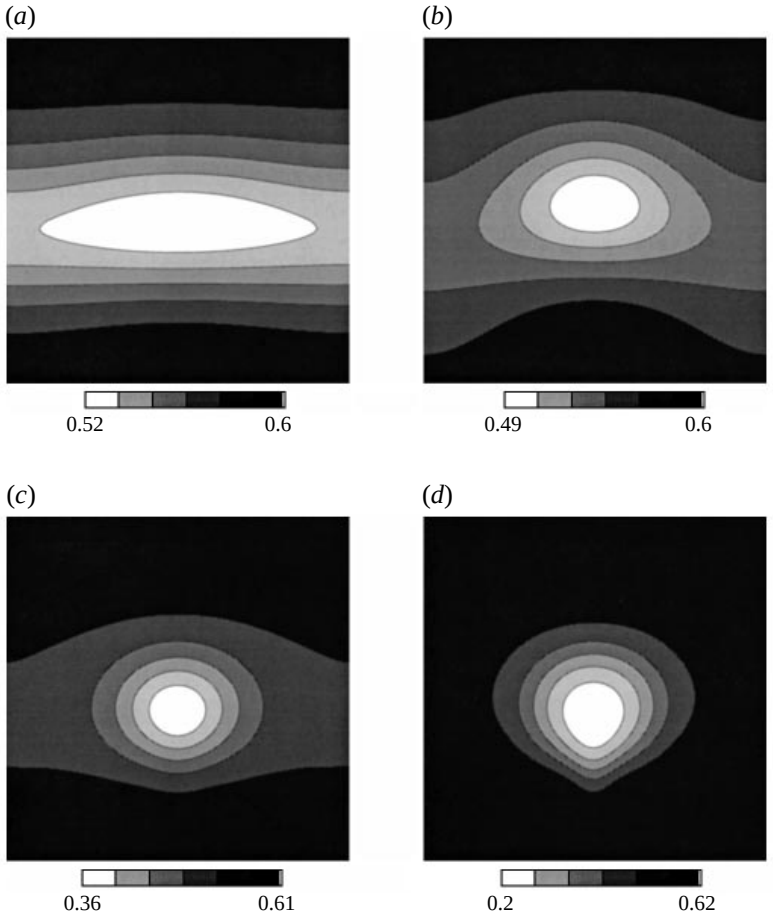

FIGURE 18. Growth of a perturbation of the 1D-TW for glass beads in water. $k_x = k_y = 0.173$. (*a*) $\hat{t} = 0$, $c = 0.200$. (*b*) $\hat{t} = 1300$ ($t = 5.24$ s), $c = 0.208$. (*c*) $\hat{t} = 3980$ ($t = 16.04$) s), $c = 0.235$, (*d*) $\hat{t} = 5370$ ($t = 21.64$ s), $c = 0.262$, $N = 18$, $M = 13$.

was then scaled so that the maximum amplitude of the ϕ-perturbation was 0.02, and was added to the 1D-TW solution to construct the initial condition for the transient simulations.

The growth of two-dimensional ϕ-structure in a periodic box with $k_x = k_y = 0.246$, for the case of 200 μm glass beads in air, is shown in figure 16. The initial condition, shown in figure 16(*a*), has a small amount of lateral structure. As time proceeds, the solution develops more lateral structure, the volume fraction of particles in the hole decreases and the gradients become steeper. The number of modes required to represent the structures accurately is indicated in the caption of this figure. The structure shown in figure 16(*d*) is virtually identical to the fully developed wave shown in figure 7. The growth of this bubble-like hole is very rapid (about 750 dimensionless time units which, for this specific example, is equal to approximately 1 s). During this growth period, the wave has travelled a distance of about 100 dimensionless units (19 cm). These are comparable to the growth times and distances required for the development of a fully developed 1D-TW from the uniform state. The evolution of ϕ-structure presented in this figure is similar to that presented in ASJ, who generated the results using an entirely different numerical scheme.

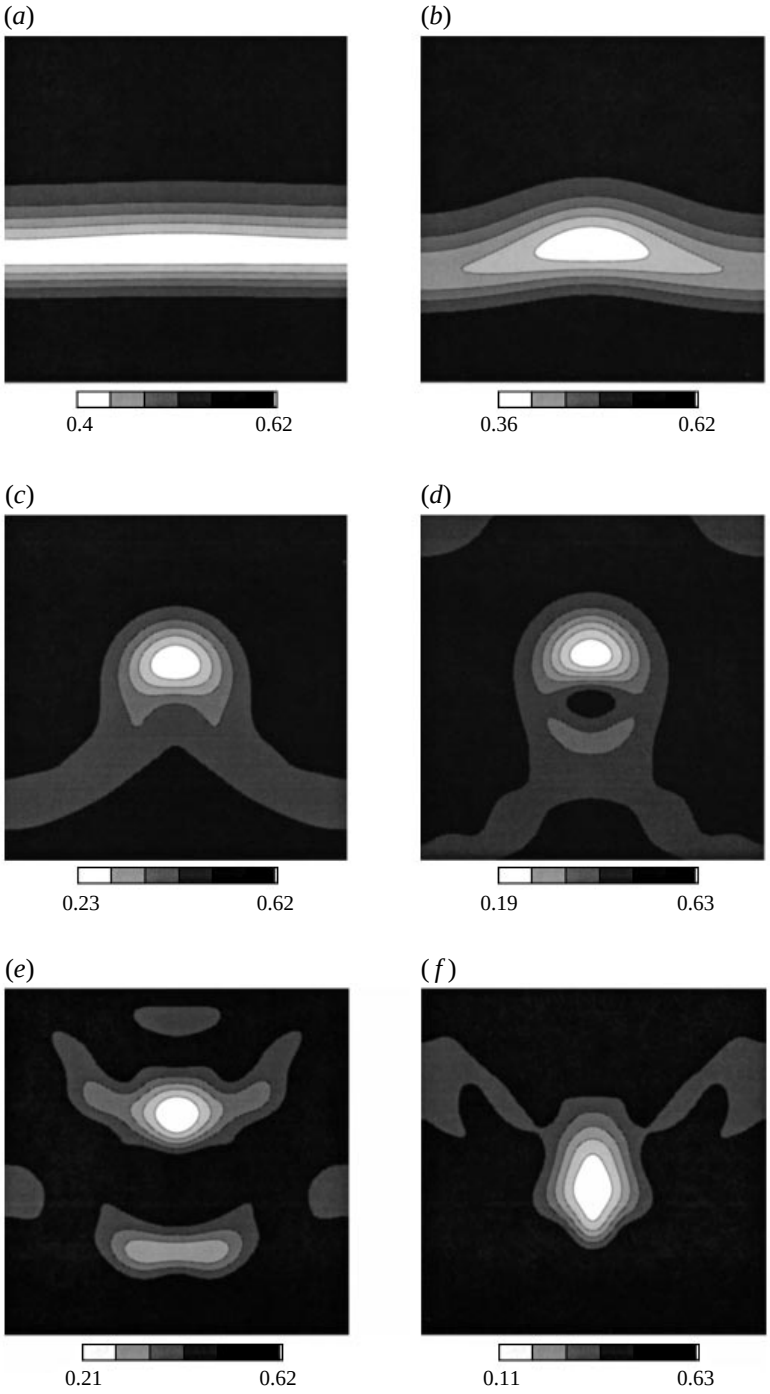

FIGURE 19. Growth of a perturbation of the 1D-TW for glass beads in water. $k_x = k_y = 0.0979$. (*a*) $\hat{t} = 0$, $c = 0.200$. (*b*) $\hat{t} = 261$ ($t = 1.05$ s), $c = 2.08$. (*c*) $\hat{t} = 385$ ($t = 1.55$ s), $c = 0.235$. (*d*) $\hat{t} = 437$ ($t = 1.76$ s), $c = 0.262$. (*e*) $\hat{t} = 561$ ($t = 2.26$ s), $c = 0.262$. (*f*) $\hat{t} = 1752$ ($t = 7.06$ s), $c = 0.262$, $N = 18$, $M = 13$.

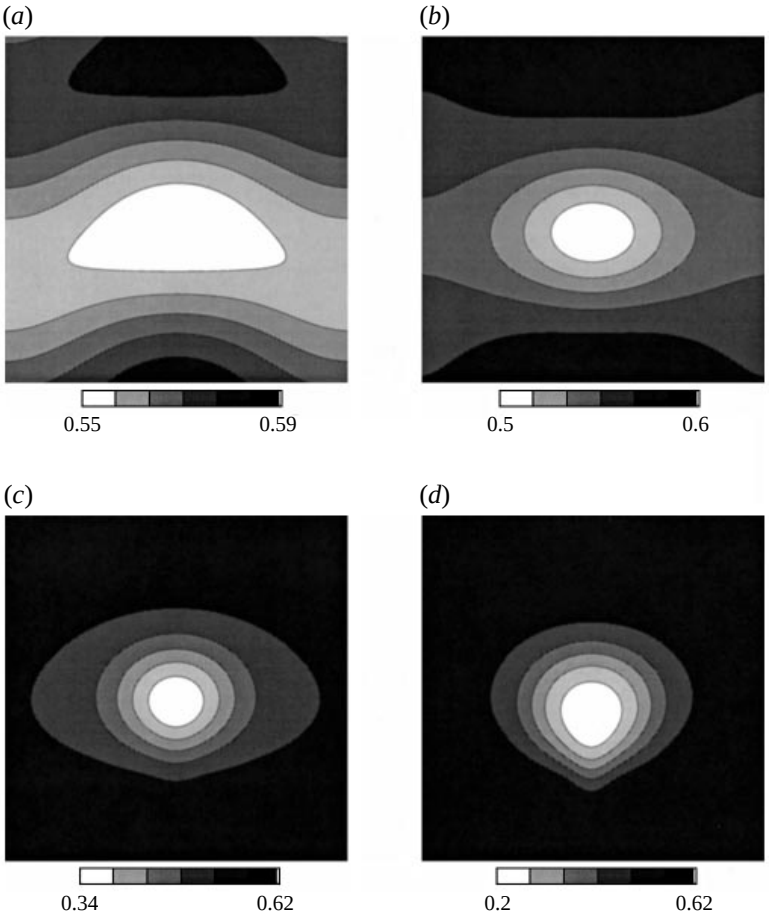

FIGURE 20. Growth of a two-dimensional perturbation of the uniform state for glass beads in water. $k_x = k_y = 0.173$. (*a*) $\hat{t} = 0$, $c = 0.201$. (*b*) $\hat{t} = 6948$ ($t = 28.0$ s), $c = 0.209$. (*c*) $\hat{t} = 10670$ ($t = 43.0$ s), $c = 0.243$. (*d*) $\hat{t} = 12655$ ($t = 51$ s), $c = 0.262$, $N = 18$, $M = 13$.

Figure 17 presents the evolution of ϕ-structure in a periodic box with $k_x = k_y = 0.188$ for the case of lead shot in water. Figure 17(*a*) indicates the initial state and the structure in figure 17(*d*) is very close to the fully developed solution (figure 9). The similarity between figures 16 and 17 is striking.

The development of ϕ-structure in a periodic box with $k_x = k_y = 0.173$ for the case of glass beads in water (corresponding to the same conditions as point Q in figure 6*c*) is shown in figure 18. Once again, the result shown in figure 18(*d*) is very close to the fully developed solution (figure 11). The manner in which the two-dimensional structure evolves in this case is clearly similar to that shown in figures 16 and 17.

Figure 19 describes the evolution of ϕ-structure in a periodic box with $k_x = k_y = 0.0979$ for the case of glass beads in water (corresponding to the same conditions as point S in figure 6*c*). The perturbed 1D-TW (figure 19*a*) buckles, and a high voidage region forms and accelerates upwards (figure 19*b*). Fluid begins to recirculate inside this high voidage region which, in turn, gives rise to the formation of a region of high ϕ at the base of the hole. By $\hat{t} = 385$ (figure 19*c*) this region of high ϕ has grown sufficiently large to disturb and break up the developing hole. The region of high voidage continues to accelerate, leaving behind arms of slower-moving voidage

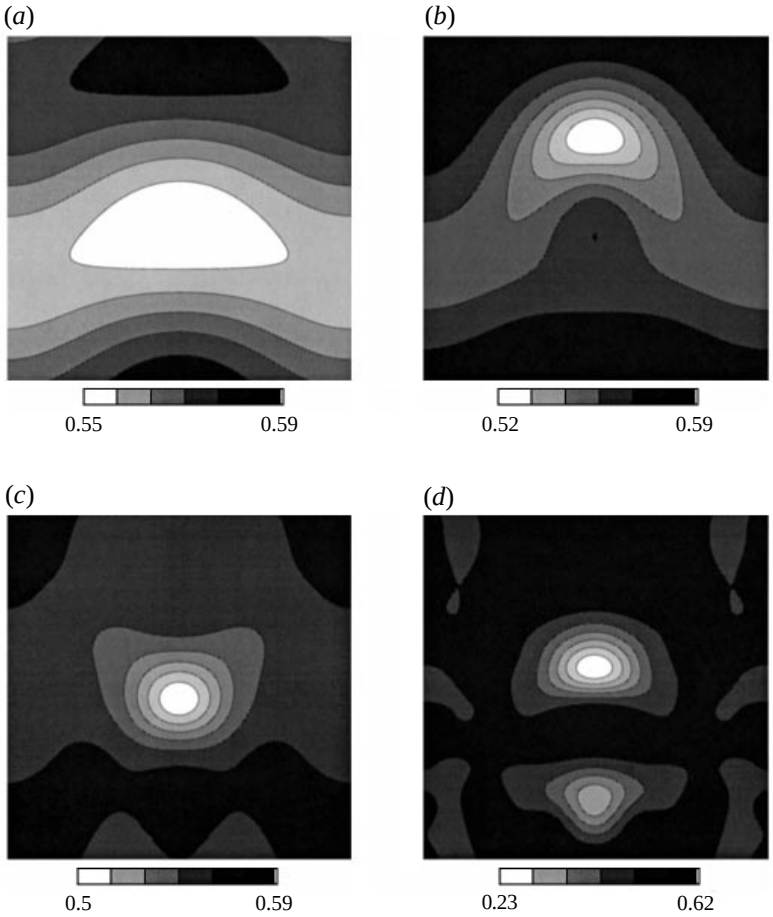

FIGURE 21. Growth of a two-dimensional perturbation of the uniform state for glass beads in water. $k_x = k_y = 0.0979$ (*a*) $\hat{t} = 0$, $c = 0.201$. (*b*) $\hat{t} = 620$ ($t = 2.5$ s), $c = 0.209$. (*c*) $\hat{t} = 1241$ ($t = 5.0$ s), $c = 0.243$. (*d*) $\hat{t} = 6452$ ($t = 26.0$ s), $c = 0.262$. $N = 18$, $M = 13$.

perturbations (figures 19(*c*) and 19(*d*)). After some time, this region of high voidage begins to interact with the slower-moving arms of the cell above (figure 19*d*) and eventually collides with it (figure 19*e*). Although the concentration of particles in the high voidage region continues to decline as time proceeds, the recirculation observed in the fluid phase is almost completely destroyed by the time $\hat{t} = 561$ (figure 19*e*). Transient integration of the averaged equations of motion for the case shown in figure 19 is computationally much more intensive than the cases described earlier, requiring very small timesteps. One of the reasons for this is that different structures in the periodic box (for example, see figure 19*e*) move at significantly different velocities through the bed. So, the strategy of performing the integration in an adaptively moving frame of reference (which permits larger timesteps to be taken) is not helpful any more. Integrating the equations up to $\hat{t}$ as high as 1752, we observed that the structure changed continually and rapidly with time, without settling down into any recognizable pattern. The solution at $\hat{t} = 1752$ (figure 19*f*) is nowhere near the fully developed structure presented in figures 13 and 14.

3.8. *Evolution of 2D-TW structure from an unstable uniform state*

We have also examined the growth of two-dimensional structures from a uniform state. In this case, while a linear stability analysis indicates that the unstable uniform state is most unstable to one-dimensional disturbances (the eigenfunction of the leading positive eigenvalue has one-dimensional structure), more than one unstable direction may exist depending on the values of k_x and k_y. The next mode to become unstable is a 'mixed mode' (whose eigenfunction has both vertical and lateral structure, see GKS1). In the case of such a two-dimensional unstable manifold for the uniform solution, we constructed initial conditions with components in both unstable directions. Through a linear stability analysis of the uniform state, the unstable one-dimensional eigenvalue and the most unstable two-dimensional eigenvalue (the 'mixed mode'), and corresponding eigenfunctions were determined. Each eigenfunction was then scaled so that the maximum amplitude of the ϕ-perturbation was 0.01, and they were added to the base state to construct the initial condition for these transient simulations.

The evolution of two-dimensional structures for the case of glass beads in water corresponding to point Q in figure 6(c) is presented in figure 20. Figure 20(a) shows the initial state and figure 20(d) is very close to the corresponding fully developed solutions (figure 11a). It is clear that the fully developed structure evolves smoothly in this case, just as it did when we started from a perturbed 1D-TW (figure 18). We simply note here that the same was found to be true for solutions corresponding to points O and P and in figures 6(a), and 6(b), representing bubble-like solutions of 'glass beads in air' and 'lead shot in water' systems (Glasser 1996).

Figure 21 corresponds to the same conditions as point S (figure 6c) of the glass beads in water system, where we see once again that the structure does not evolve in a smooth manner. In this example we have followed the growth for a much longer time (when compared to that shown in figure 19). Yet the structure is nowhere near the corresponding fully developed structure.

4. Discussion

Anderson *et al.* (1995) examined the growth of two-dimensional structures in bubbling and non-bubbling systems through transient integration of the averaged equations of motion assuming spatial periodicity. They demonstrated that apparently stable bubble-like solutions evolved smoothly in a bed of glass beads fluidized by air. In contrast, no such structures developed in a bed of glass beads fluidized by water. They went on to conclude that the equations of motion with simple and credible closure relations contained the essential physics needed to distinguish between bubbling and non-bubbling systems. The present study seeks a more specific understanding of the origin of this distinction.

We have established that both bubbling and non-bubbling systems manifest identical bifurcation hierarchy. In both cases, fully-developed two-dimensional travelling wave solutions of high amplitude have bubble-like holes, and these solutions are linearly stable. Furthermore, recirculation of fluid is observed in both cases, with fluid travelling upward (in the wave frame) in the centre of the hole. In some instances, this upward velocity is much smaller than the terminal velocity of the particle, while in others, it can exceed the terminal velocity. In the former situation, the particles accelerate as they enter the hole through its roof and decelerate as they exit the hole at the bottom. We have shown that disturbances of the unstable base state as well as of the unstable 1D-TW will evolve smoothly to these fully developed states.

In the latter situation, the particles experience an intermediate stage of deceleration and re-acceleration. These locally stable fully developed two-dimensional states, however, do not evolve smoothly (i.e. are not accessible) from either the base or the 1D-TW states. Small perturbations of the base or 1D-TW states do give rise to transient two-dimensional structures, which neither approach the stable 2D-TWs nor settle down to stationary patterns on the (quite extensive) timescale of our simulations. It is tempting to ascribe the 'inaccessibility' of these bubble-like structures to differences in growth rates between the primary and secondary instabilities (ASJ). This difference does correlate with non-bubbling systems, but does not tell the entire story: while high-amplitude two-dimensional solutions are not accessible to simulations starting close to the unstable base state or the 1D-TW, small-amplitude two-dimensional solutions are indeed accessible even in the presence of such a pronounced difference in timescales between the primary and secondary instabilities. During the growth of high-amplitude solutions, a bubble-like structure may form initially, but it breaks up sooner or later (as noted already in ASJ). The formation of such a transient bubble-like voidage structure in a non-bubbling liquid-fluidized bed has indeed been observed experimentally by El-Kaissy & Homsy (1976) and Didwania & Homsy (1981). Local stability and bifurcation calculations cannot explain such a (global) transient feature of the flow; the transients do not appear to approach any obvious (tertiary, unstable and possibly time-dependent) additional solution branches, even though such separatrices must be present. The calculations quickly get very computer-intensive owing to the generation of a wide range of spatial and temporal scales. Even though these transients do not eventually 'settle down', they do reveal a physically relevant, albeit transient, bubble breakup mechanism, discussed by ASJ. We propose that the appearance of a fully developed solution (in a numerical bifurcation analysis) in which the particles experience an intermediate stage of deceleration and re-acceleration can be used as an identification mark of non-bubbling systems. This classification will correctly group the cases of 200 μm glass beads in air, and 1 mm lead shot in water as bubbling systems. The system of 1 mm glass beads in water will be labelled by this criterion as non-bubbling. Adopting this classification scheme, we sought to identify the key dimensionless group which distinguishes bubbling and non-bubbling systems (see Glasser 1996).

The equations of motion contain, six independent dimensionless groups, δ, γ, ϕ_c (or α), Ω, n and r. We simply note here that γ, ϕ_c (or α), n and r are not critical from the point of view of distinguishing bubbling and non-bubbling systems. For example, it was found through numerical bifurcation analysis (Glasser 1996) that a bubbling system cannot be transformed into a non-bubbling system by changing ϕ_c (or, equivalently, α). The effect of δ on the bifurcation structure was examined by holding the values of the dimensionless parameters α, γ, Ω, n and r, to be the same as those in the first column of table 1 and changing only δ to 0.5. This change will necessarily alter the value of ϕ_c, but this change is only small (ϕ_c is now 0.58). It was found that the family of fully developed 2D-TW solutions (computed for $\phi_0 = 0.577$, which is slightly smaller than ϕ_c) did not develop features indicative of non-bubbling systems (Glasser 1996). This suggests that δ is not a critical parameter.

It is well documented that beds of 1 mm glass beads fluidized by water do not bubble, while beds of 1 mm lead shot fluidized by water are known to bubble. Clearly, the density ratio has influenced the bed behaviour in a significant way. Thus, our finding that δ is not a critical parameter appears at first sight to be inconsistent with experimental observations, but it is not. It is important to recognize that in such experiments, one has not only changed the parameter δ appearing in the model, but

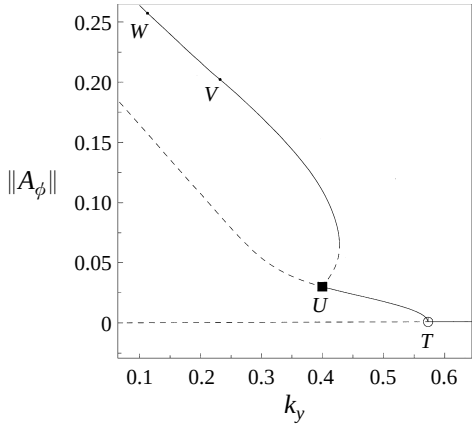

FIGURE 22. Bifurcation diagrams for parametric study showing the uniform state and one- and two-dimensional travelling wave solutions. $k_x = k_y$.

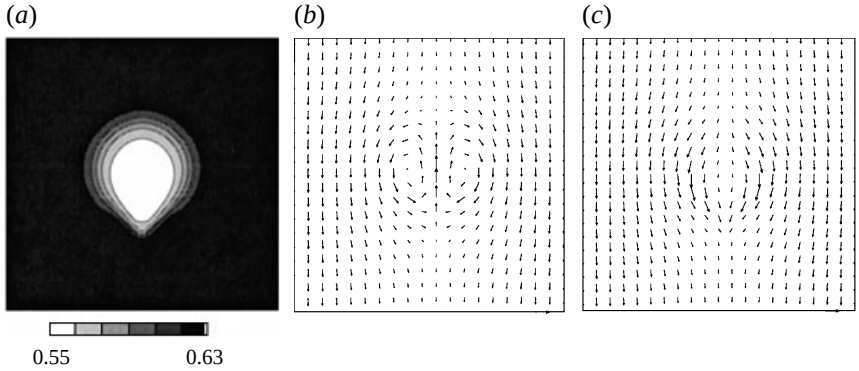

FIGURE 23. Two-dimensional travelling wave solution, corresponding to point W in figure 22. $k_x = k_y = 0.11$, $N = 24$, $M = 16$. $c = 0.442$. (*a*) Volume fraction of solids. (*b*) Vector plot of gas velocity (longest vector $= 0.728 v_t$). (*c*) Vector plot of solids velocity (longest vector $= 0.837 v_t$).

also other parameters (most notably, Ω) (see columns 2 and 3 of table 1). Our analysis reveals that changing δ, while holding Ω constant, does not produce qualitative changes.

Thus, the key parameter which separates bubbling and non-bubbling systems must by Ω. It is clear from table 1 that bubbling systems are characterized by large values of Ω, while its value for the non-bubbling system is noticeably smaller. In order to verify that a bubbling system can be changed into a non-bubbling system by simply decreasing Ω, consider a system having the same values of α, δ, γ, n and r as in column 1 of table 1, and $\Omega = 3.79$. The bifurcation diagram for this system with $\phi_0 = 0.57$ is shown in figure 22. The fully-developed solutions for two points V (not shown) and W (figure 23) on the 2D-TW branch of this figure are qualitatively similar to those corresponding to points Q and S of figure 6(*c*) (see figures 11 and 13). Thus, we can state with some confidence that systems for which $\Omega = O(1)$ can be classified as non-bubbling, while those for which $\Omega = O(100)$ will bubble.

Note that in the example presented in figures 22 and 23, $\delta \ll 1$ so that we are still looking at a gas-fluidized bed. Furthermore, decreasing Ω is physically equivalent to decreasing the particle size. Thus, the present analysis suggests that gas-fluidized beds

of 'small' non-cohesive particles will not bubble. There does not appear to be any experimental evidence to support this finding. It would be of interest to investigate experimentally the fluidization characteristics of small non-cohesive particles (of various diameters) to test our finding. It should be remarked that air-fluidized beds of fluid catalytic cracking (FCC) particles, with a mean diameter of about 75 μm, do bubble (Tsinontides & Jackson 1993). However, it has been shown that a bed of FCC particles manifests a yield stress and a pronounced hysteresis during fluidization/defluidization cycles (Tsinontides & Jackson 1993). We conjecture that bubbling observed in this system is a consequence of the cohesive interactions, and that in the absence of cohesive interactions air-fluidized beds of particles of this size may not bubble easily.

The parameter Ω contains the viscosity parameter A whose value is not precisely known. Note that we had assumed that the three physical systems described in table 1 have the same value of A. This assumption is, of course, irrelevant in our analysis of the equations in a dimensionless form, which revealed Ω as the key parameter. Nevertheless, the value assumed for A will impact the value of Ω assigned to a given physical system which, in turn, can affect how this system is classified. It is therefore important to express A in terms of suitable length, velocity and density scales characterizing the fluidized suspension. From a dimensional argument, it appears natural to write $A \approx K\rho_s v_t d_p$, where K is a proportionality constant. Schügerl, Merz & Fetting (1961) have measured viscosities of gas-fluidized beds using a Couette cylinder viscometer and their results do support such a scaling. It is interesting to assume this scaling and examine the predicted consequences. Inserting this relation into the definition of Ω, we get

$$\Omega = B\left(\frac{v_t^2}{gd_p}\right)^{1/2} \equiv B\,Fr_t^{1/2}, \tag{11}$$

where $B = K^{-1/2}$ and Fr_t is a Froude number based on the terminal velocity.

Wilhelm & Kwauk (1948) proposed empirically a Froude number criterion for distinguishing between bubbling and non-bubbling systems:

$$Fr_m \gg 1 \Rightarrow \text{bubbling}, \quad Fr_m \ll 1 \Rightarrow \text{non-bubbling},$$

where $Fr_m = (u_m^2/gd_p)$ and u_m is the relative velocity between the fluid and particle phases under conditions of minimum fluidization. Early theoretical efforts in this field tried to justify this Froude number criterion for distinguishing between bubbling and non-bubbling systems through linear stability analysis of the uniform state by treating bubbling as a manifestation of loss of stability of the state of uniform fluidization and absence of bubbling as a sign of stability of the uniform state (see ASJ for further discussion of this point). Experiments by Anderson & Jackson (1969) and El-Kaissy & Homsy (1976) exposed this approach as fallacious. The present work and the earlier work by ASJ have revealed clearly that the distinction between bubbling and non-bubbling systems is intimately linked with high-amplitude solutions; yet, it appears that this differentiation may indeed be expressed in terms of a Froude number criterion.

Harrison *et al.* (1961) pointed out that bubbles cannot be observed experimentally unless they are considerably larger than the particle size, and proposed a criterion for distinguishing between bubbling and non-bubbling systems on the basis of largest stable bubble size (D_e). They examined the stability of spherical cap bubbles in a fluidized bed and concluded that large bubbles can be stable in most gas-fluidized beds, while the largest size of stable bubble in most liquid-fluidized beds is comparable to the

size of the particles in the bed. Their analysis revealed that D_e/d_p is proportional to Fr_m, thus providing a physical justification for the empirical observation of Wilhelm & Kwauk (1948).

Our computational analysis suggests that fluidized beds with $\Omega \gg 10$ will bubble, while those with $\Omega \ll 10$ are not likely to. Assuming B in (11) to be $O(1)$, we find that bubbling systems are characterized by $Fr_t \gg 100$, while for non-bubbling $Fr_t \ll 100$. Noting that u_m is typically a tenth of v_t for the cases we examined, one recovers the same criterion deduced experimentally by Wilhelm & Kwauk (1948).

The values of B corresponding to the values of A assumed in our simulations are listed in table 1. It can be seen that B is approximately a constant (of $O(1)$) for the glass beads in air and the glass beads in water cases. However, the value of B for lead shot fluidized by water is $O(10)$. This highlights that definitive classification of physical systems on the basis of the equations of motion analysed in the present study can be made only when one can characterize the particle phase viscosity quantitatively. In any case, we know now that these equations do contain the essential physics needed to separate bubbling and non-bubbling behaviour and that the controlling parameter is Ω.

This work has been partially supported by the National Science Foundation, the Mobil Foundation, the Exxon Education Foundation and ARPA/ONR. The computational work was carried out through a grant of time on a CRAY C90 from the Pittsburgh Supercomputing Center. We would like to acknowledge the considerable help and advice we received from Karl Anderson, Manfred Göz and Professor Roy Jackson over the course of this work.

REFERENCES

Anderson, K. G., Sundaresan, S. & Jackson, R. 1995 Instabilities and the formation of bubbles in fluidized beds. *J. Fluid Mech.* **303**, 327–366 (referred to herein as ASJ).

Anderson, T. B. & Jackson, R. 1967 Fluid mechanical description of fluidized beds. Equations of motion. *Ind. Engng Chem. Fund.* **6**, 527–539.

Anderson, T. B. & Jackson, R. 1968 Fluid mechanical description of fluidized beds. Stability of the state of uniform fluidization. *Ind. Engng Chem. Fund.* **7**, 12–21.

Anderson, T. B. & Jackson, R. 1969 Fluid mechanical description of fluidized beds. Comparison of theory and experiment. *Ind. Engng Chem. Fund.* **8**, 137–144.

Batchelor, G. K. 1988 A new theory of the instability of a uniform fluidized bed. *J. Fluid Mech.* **193**, 75–110.

Dankworth, D. C. & Sundaresan, S. 1991 Time-dependent flow patterns arising from the instability of uniform fluidization. Presentation at *Symp. Mech. Fluidized Beds, 1–4 July 1991, Stanford University* (see also *J. Fluid Mech.* **236**, 477–495).

Didwania, A. K. & Homsy, G. M. 1981 Flow regimes and flow transitions in liquid fluidized beds. *Intl J. Multiphase Flow* **7**, 563–580.

El-Kaissy, M. M. & Homsy, G. M. 1976 Instability waves and the origin of bubbles in fluidized beds. I: Experiments. *Intl J. Multiphase Flow* **2**, 379–395.

Fanucci, J. B., Ness, N. & Yen, R-H. 1979 On the formation of bubbles in gas-particulate fluidized beds. *J. Fluid Mech.* **94**, 353–367.

Foscolo, P. U. & Gibilaro, L. G. 1984 A fully predictive criterion for the transition between particulate and aggregative fluidization. *Chem. Engng Sci.* **39**, 1667–1675.

Garg, S. K. & Pritchett, J. W. 1975 Dynamics of gas fluidized beds. *J. Appl. Phys.* **46**, 4493–4500.

Gear, C. W. 1971 Simultaneous numerical solution of differential-algebraic equations. *IEEE Trans. Circuit Theory* CT **18**, 89–95.

Gidaspow, D., Syamlal, M. & Seo, Y. C. 1986 Hydrodynamics of fluidization: supercomputer generated *vs.* experimental bubbles. *J. Powder and Bulk Solids Tech.* **10**, 19–23.

Glasser, B. J. 1996 One- and two-dimensional traveling wave solutions in fluidized beds. PhD dissertation, Princeton University.

Glasser, B. J., Kevrekidis, I. G. & Sundaresan, S. 1996 One- and two-dimensional travelling wave solutions in gas-fluidized beds. *J. Fluid Mech.* **306**, 183–221 (referred to herein as GKS1).

Göz, M. F. 1992 On the origin of wave patterns in fluidized beds. *J. Fluid Mech.* **240**, 379–404.

Göz, M. F. 1993 Bifurcation of plane voidage waves in fluidized beds. *Physica* D **65**, 319–351.

Göz, M. F. 1995 Transverse instability of plane wavetrains in gas-fluidized beds. *J. Fluid Mech.* **303**, 55–82.

Harris, S. E. & Crighton, D. G. 1994 Solitons, solitary waves, and voidage disturbances in gas-fluidized beds. *J. Fluid Mech.* **266**, 243–276.

Harrison, D., Davidson, J. F. & De Kock, J. W. 1961 On the nature of aggregative and particulate fluidisation. *Trans. Inst. Chem. Engrs* **39**, 202–211.

Hernández, J. A. & Jiménez, J. 1991 Bubble formation in dense fluidized beds. In *Proceedings of NATO Advanced Research Workshop on the Global Geometry of Turbulence* (ed. J. Jiménez), pp. 133–142. Plenum.

Jackson, R. 1963 The mechanics of fluidized beds. I: The stability of the state of uniform fluidization. *Trans. Inst. Chem. Engrs* **41**, 13–21.

Kuipers, J. A. M., Prins, W. & Van Swaaij, W. P. M. 1991 Theoretical and experimental bubble formation at a single orifice in a two-dimensional gas-fluidized bed. *Chem. Engng Sci.* **46**, 2881–2894.

Kunii, D. & Levenspiel, O. 1991 *Fluidization Engineering*. Butterworth–Heineman.

Mutsers, S. M. P. & Rietema, K. 1977 The effect of interparticle forces on the expansion of a homogeneous gas-fluidized beds. *Powder Tech.* **18**, 239–248.

Needham, D. J. & Merkin, J. H. 1983 The propagation of a voidage disturbance in a uniform fluidized bed. *J. Fluid Mech.* **131**, 427–454.

Needham, D. J. & Merkin, J. H. 1986 The existence and stability of quasi-steady periodic voidage waves in a fluidized beds. *Z. angew Math. Phys.* **37**, 322–339.

Petzold, L. 1982 Differential/algebraic equations are not ODE's. *SIAM J. Sci. Stat. Comput.* **3**, 367–384.

Pigford, R. L. & Baron, T. 1965 Hydrodynamic stability of a fluidized bed. *Ind. Engng Chem. Fund.* **4**, 81–87.

Pritchett, J. W., Blake, T. R. & Garg, S. K. 1978 A numerical model of gas fluidized beds. *AIChE Symp. Ser. No. 176* **74**, 134–148.

Richardson, J. F. & Zaki, W. N. 1954 Sedimentation and fluidization: Part I. *Trans. Inst. Chem. Engrs* **32**, 35–53.

Schügerl, K., Merz, M. & Fetting, F. 1961 Rheologische Eigenschaften von gasdurchströmten Fliessbettsystemen. *Chem. Engng Sci.* **15**, 1–38.

Syamlal, M. & O'Brien, T. J. 1989 Computer simulation of bubbles in a fluidized bed. *AIChE Symp. Ser. No. 270* **85**, 22–31.

Tsinontides, S. & Jackson, R. 1993 The mechanics of gas fluidized beds with an interval of stable fluidization. *J. Fluid Mech.* **255**, 237–274.

Wilhelm, R. H. & Kwauk, M. 1948 Fluidization of solid particles. *Chem. Engng Progr.* **44**, 201–218.